The Arabidopsis Synaptotagmin1 Is Enriched in Endoplasmic Reticulum-Plasma Membrane Contact Sites and Confers Cellular Resistance to Mechanical Stresses[1][OPEN]

Jessica Pérez-Sancho, Steffen Vanneste, Eunkyoung Lee, Heather E. McFarlane, Alicia Esteban del Valle, Victoriano Valpuesta, Jiří Friml, Miguel A. Botella*, and Abel Rosado*

Instituto de Hortofruticultura Subtropical y Mediterránea, Universidad de Málaga-Consejo Superior de Investigaciones Científicas, Departamento de Biología Molecular y Bioquímica, Facultad de Ciencias, Universidad de Málaga, 29071 Malaga, Spain (J.P.-S., A.E.d.V., V.V., M.A.B., A.R.); Department of Plant Systems Biology, Vlaams Instituut voor Biotechnologie, 9052 Ghent, Belgium (S.V., J.F.); Department of Plant Biotechnology and Bioinformatics, Ghent University, 9052 Ghent, Belgium (S.V., J.F.); Department of Botany, Faculty of Sciences, University of British Columbia, Vancouver, Canada V6T 1Z4 (E.L., H.E.M., A.R.); and Max Planck Institute for Molecular Plant Physiology, 14476 Potsdam, Germany (H.E.M.)

ORCID IDs: 0000-0002-8867-1831 (M.A.B.); 0000-0001-8674-1050 (A.R.).

Eukaryotic endoplasmic reticulum (ER)-plasma membrane (PM) contact sites are evolutionarily conserved microdomains that have important roles in specialized metabolic functions such as ER-PM communication, lipid homeostasis, and Ca^{2+} influx. Despite recent advances in knowledge about ER-PM contact site components and functions in yeast (*Saccharomyces cerevisiae*) and mammals, relatively little is known about the functional significance of these structures in plants. In this report, we characterize the Arabidopsis (*Arabidopsis thaliana*) phospholipid binding Synaptotagmin1 (SYT1) as a plant ortholog of the mammal extended synaptotagmins and yeast tricalbins families of ER-PM anchors. We propose that SYT1 functions at ER-PM contact sites because it displays a dual ER-PM localization, it is enriched in microtubule-depleted regions at the cell cortex, and it colocalizes with Vesicle-Associated Protein27-1, a known ER-PM marker. Furthermore, biochemical and physiological analyses indicate that SYT1 might function as an electrostatic phospholipid anchor conferring mechanical stability in plant cells. Together, the subcellular localization and functional characterization of SYT1 highlights a putative role of plant ER-PM contact site components in the cellular adaptation to environmental stresses.

Land plants are sessile organisms that are persistently challenged by physicomechanical forces that arise from the external environment. Some of the most common mechanical stimuli perceived by plants, collectively termed thigmostimuli (the Greek prefix thigmo means touch), are those induced by gradients in pressure (e.g. wind or tidal flows), by the gravity vector (e.g. ice and snow accumulation), or by direct impact with inanimate objects and/or living organisms (e.g. raindrops, hailstones, insects, canopy rubbing; Telewski, 2006). Mechanical stresses are not only exerted by the environment but are also intrinsic to the biophysics of plant growth (Landrein and Hamant, 2013). For instance, plants experience progressive mechanical self-loading as they increase in size or bear fruit (Almeras et al., 2004), intricate stress patterns are generated by different expansion rates between particular plant tissues (Mirabet et al., 2011; Sampathkumar et al., 2014), and plant cells, which are physically restrained by a rigid cell wall, generate turgor pressure characterized by circumferential tensile forces and radial compressive forces toward the plasma membrane (Telewski, 2006).

[1] This work was supported by a Formación del Personal Investigador Fellowship from the Ministerio de Economía y Competitividad (FPI-BES 2012-052324 to J.P.-S), the Ministerio de Ciencia e Innovación (cofinanced by the European Regional Development Fund; grant no. BIO2011-23859), the Consejería de Innovación Ciencia y Empresa-La Junta de Andalucía (cofinanced by the European Regional Development Fund; grant no. P07-CVI-03021 to M.A.B), a postdoctoral research fellowship of the Research Foundation-Flanders (to S.V.), and the Natural Sciences and Engineering Research Council of Canada Discovery (grant no. RGPIN-2014-06468) and Canada Research Chairs programs (to A.R.).

* Address correspondence to abel.rosado@botany.ubc.ca and mabotella@uma.es.

The author responsible for distribution of materials integral to the findings presented in this article in accordance with the policy described in the Instructions for Authors (www.plantphysiol.org) is: Abel Rosado (abel.rosado@botany.ubc.ca).

J.P.-S., S.V., E.L., H.E.M., and A.R. performed most of the experiments; A.E.d.V. provided technical assistance to J.P.-S. and A.R.; M.A.B., A.R., S.V., H.E.M., and J.P.-S. designed the experiments and analyzed the data; M.A.B. and A.R. conceived the project and wrote the article; V.V., J.F., J.P.-S., S.V., and H.E.M. supervised and complemented the writing.

[OPEN] Articles can be viewed without a subscription.

www.plantphysiol.org/cgi/doi/10.1104/pp.15.00260

Under mechanical stresses, different cell types, including meristematic, expanding, and fully differentiated cells, undergo physiological changes based on the sensing and integration of various mechanical signals (Monshausen and Haswell, 2013). Although it is well established that plants sense and respond to mechanical cues, our understanding of the various molecular mechanisms by which this is accomplished is limited, and most of our knowledge relies on comparisons with mechanosensors and transduction pathways identified in *Escherichia coli* and mammalian cells (Arnadóttir and Chalfie, 2010). Currently, two nonmutually exclusive mechanosensing models, namely, the ion channel and the tensegrity models, coexist in the plant literature. In the ion channel model, plant homologs of the bacterial mechanosensitive channel of small conductance and putative stretch-activated Ca^{2+}-permeable channels are gated in response to mechanical forces and trigger a signaling cascade through the rapid influx of extracellular Ca^{2+} toward the cytosol (Arnadóttir and Chalfie, 2010; Jensen and Haswell, 2012; Sukharev and Sachs, 2012; Kurusu et al., 2013). In the tensegrity model, plant cells operate as self-supporting structures stabilized by a dynamic prestress state in which all elements are in isometric tension (Fuller, 1961). In such a structure, the mechanical disturbance of any individual element allows stress signals to propagate and be transduced at relatively distant locations (Ingber, 2008). Thus, the mechanically stable cell walls provide structural support, and the constant remodeling of the underlying cytoskeleton in response to mechanical disturbances acts as a tensegrity sensor (Komis et al., 2002; Berghöfer et al., 2009; Nick, 2013).

In this article, we characterize the Arabidopsis (*Arabidopsis thaliana*) type I anchor Synaptotagmin1 (SYT1/SYTA/NTMC2T1.1 [hereafter SYT1]; Craxton, 2010; Yamazaki et al., 2010; Lewis and Lazarowitz, 2010) as an important component required to withstand mechanical stress in plant cells. SYT1 belongs to a five-member family in Arabidopsis and shares a common modular structure with different members of the mammalian extended synaptotagmins (E-Syts) and yeast (*Saccharomyces cerevisiae*) tricalbins families of organelle tethers (Manford et al., 2012; Fig. 1A; Supplemental Fig. S1). These proteins act as molecular bridges between the ER and the PM at sites where both cellular membranes are in close proximity, called ER-PM contact sites. These specialized microdomains carry out important roles in organelle communication, lipid and Ca^{2+} homeostasis, and intracellular signaling in animal and yeast cells (Toulmay and Prinz, 2011; Helle et al., 2013; Prinz, 2014). In plants, these ER-PM contact sites have been morphologically described for decades (Staehelin, 1997), but their physiological roles have not been thoroughly characterized. Furthermore, the identity of molecular components at these sites has remained elusive until the recent characterization of the ER-PM localized Vesicle-Associated Protein27-1 (VAP27) and NETWORKED 3C (NET3C) markers in Arabidopsis (Wang et al., 2014).

In previous reports, SYT1 has been described as an essential component for PM integrity maintenance, especially under conditions of high potential for membrane disruption such as freezing or salt stresses (Schapire et al., 2008, 2009; Yamazaki et al., 2008). In these reports, SYT1 was proposed to act as a Ca^{2+}-dependent regulator of

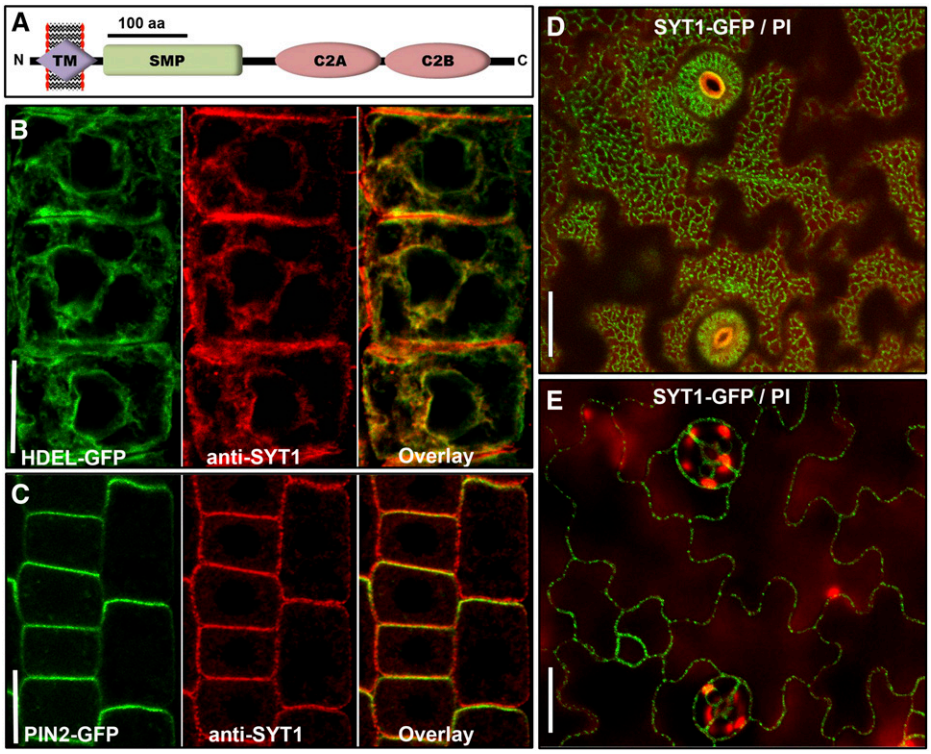

Figure 1. SYT1 displays dual endoplasmic reticulum (ER)-plasma membrane (PM) localization. A, Schematic representation of the SYT1 structure and functional domains. TM, Transmembrane domain; SMP, synaptotagmin-like-mitochondrial-lipid binding domain; C2A and C2B, Ca^{2+} and phospholipid binding domains. B and C, Coimmunolocalization of the endogenous SYT1 and the ER marker HDEL-GFP (B) or the PM marker PIN2-GFP (C) in 5-d-old root epidermal cells. Scale bars = 10 μm. D and E, Subcellular localization of the SYT1proSYT1-GFP marker (SYT1-GFP) in leaves. Images were acquired at the cortical (D) or equatorial regions (E) of 8-d-old leaf epidermal cells. Costaining with propidium iodide (PI) was used to facilitate the visualization of the cortical regions. Scale bars = 20 μm.

membrane fusion, in analogy to the classical animal SYTs that mediate Ca^{2+}-triggered vesicle fusion during neurotransmission (Carr and Munson, 2007). Another report highlighted a role for SYT1 in viral spreading from cell to cell (Lewis and Lazarowitz, 2010). The recent characterization of mammalian E-Syts in stress tolerance (Herdman et al., 2014) and the phylogenetic relationships of tricalbins and E-Syts with SYT1 (Craxton, 2010; Yamazaki et al., 2010) led us to hypothesize that SYT1 could be a functional ortholog of E-Syts and tricalbins in plants. Consistently, we found that it is localized in specific ER-PM subdomains in cortical cytoskeleton-depleted regions, it colocalizes with the VAP27 marker, and it anchors negatively charged phospholipids through its PM-targeted C2 domains. Additionally, we show that SYT1 loss of function causes mechanical instability at the tissue and cellular level without altering the gross ER morphology. Based on these findings, we conclude that SYT1 acts at ER-PM contact sites as part of structural platforms adjacent to the cortical cytoskeleton that are required for mechanical stress tolerance in Arabidopsis.

RESULTS

The Arabidopsis SYT1 Localizes at the ER and the PM and Accumulates at ER-PM Contact Sites

SYT1 contains a modular structure similar to ER-PM tether proteins such as E-Syts and tricalbins (Craxton, 2010; Yamazaki et al., 2010), proteins that are localized at specific ER-PM subdomains (Giordano et al., 2013; Helle et al., 2013; Prinz, 2014). Moreover, cell biological and biochemical analyses have reported SYT1 being at the ER, PM, and plasmodesmata (Schapire et al., 2008; Lewis and Lazarowitz, 2010; Yamazaki et al., 2010). To unequivocally establish the SYT1 subcellular localization, we developed new polyclonal anti-$SYT1_{244\text{-}541}$ antibodies (hereafter, anti-SYT1), and demonstrated their specificity by the absence of signal in the null *syt1-2* mutant (hereafter, *syt1*) via western blot and immunolocalization (Supplemental Fig. S1). Next, we performed immunolocalization analyses in transgenic Arabidopsis lines expressing the GFP-tagged ER retention peptide HDEL (HDEL-GFP), and the PM markers PIN-FORMED2 (PIN2-GFP), BRASSINOSTEROID INSENSITIVE1 (BRI1-GFP), and PLASMA MEMBRANE INTRINSIC PROTEIN 2A (PIP2A-GFP). As shown in Figure 1B, the anti-SYT1 perinuclear signal colocalized with HDEL-GFP, confirming the broad ER localization of SYT1. Interestingly, at the cell cortex, the anti-SYT1 signal was characterized by a punctate pattern that was closely associated with HDEL-GFP but did not colocalize (Supplemental Fig. S1). Remarkably, in those cortical regions, the anti-SYT1 signal colocalized with PM markers PIN2-GFP, BRI1-GFP, and PIP2A-GFP (Fig. 1C; Supplemental Fig. S2), suggesting a dual ER-PM localization. To analyze the SYT1 subcellular localization in leaf epidermal cells, we generated transgenic Arabidopsis lines expressing a C-terminal translational fusion of GFP to SYT1 (*SYT1proSYT1-GFP*; hereafter, SYT1-GFP). At the cell cortex, the SYT1-GFP marker appeared as a reticulate network of beads and strings (Fig. 1D) that was clearly different from the classical network of sheets and interconnected tubules observed in the luminal ER marker HDEL-GFP and the GFP-tagged membrane-associated ER marker SECRETORY 12P-LIKE-GFP (Supplemental Fig. S3). At the equatorial plane, the SYT1-GFP marker appeared as a punctuate signal at the cell periphery (Fig. 1E), and signal movement through transvacuolar strands was observed (Supplemental Movie S1). Transient colocalization in *Nicotiana benthamiana* of a Red Fluorescent Protein (RFP)-tagged SYT1 fused to its endogenous promoter(SYT1proSYT1-RFP) with the ER-targeted yellow cameleon 4.60 (Iwano et al., 2009) showed that the SYT1 signal was enriched at specific ER subdomains (Supplemental Fig. S3). A high-resolution subcellular localization for SYT1 was obtained by immunogold Transmission Electron Microscopy (immunoTEM) of high-pressure frozen, freeze-substituted wild-type roots probed with the anti-SYT1 antibody. Similar to previous immunoTEM results (Schapire et al., 2008), the anti-SYT1 signal was observed at both the ER and PM (Supplemental Fig. S4). However, the use of more specific and sensitive antibodies together with the better structural preservation of the high-pressure frozen samples enabled us to observe an enrichment of the anti-SYT1 signal in regions where the cortical ER was in close apposition to the PM (Fig. 2A),

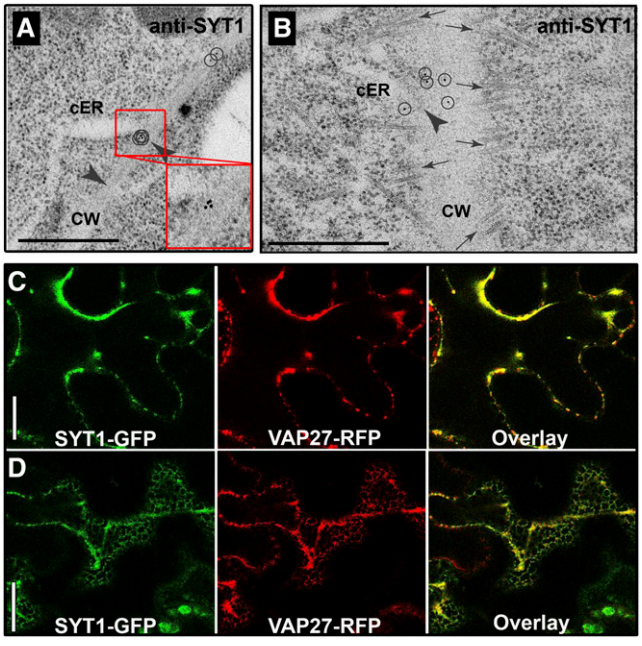

Figure 2. SYT1 is enriched at ER-PM contact sites. A and B, Immuno-TEM of high-pressure frozen, freeze-substituted wild-type roots probed with anti-SYT1 and a 10-nm gold-conjugated secondary antibody. Circles, Gold particles; cER, cortical ER; CW, cell wall; arrowheads, ER-PM contact sites. Scale bar = 500 nm. C and D, Transient colocalization of the SYT1-GFP and VAP27-RFP markers in *N. benthamiana*. The equatorial (C) and cortical planes (D) are shown. Scale bars = 40 μm.

and between cortical microtubule bundles (Fig. 2B). Since the SYT1 localization at the ER-PM interface strongly resembled that of the recently reported Arabidopsis VAP27 and NET3C ER-PM markers (Wang et al., 2014), we next performed transient colocalization studies using the RFP-tagged VAP27 fused to the Ubiquitin-10 promoter (UBQ10proVAP27-RFP) and SYT1proSYT1-GFP markers in *N. benthamiana* leaves. As shown in Figure 2, C and D, the markers colocalized to a great extent in both intracellular and cortical regions of the cell. Together, these data strongly suggest that SYT1 is enriched at ER-PM contact sites, a feature shared with the E-Syts and tricalbins in animals and yeast, respectively.

The SYT1-Labeled ER-PM Contact Sites Are Predominantly Stationary

Once we determined that SYT1 populations with different subcellular localizations coexist in plant cells, we analyzed the dynamics of SYT1-GFP using time-lapse and fluorescence recovery after photobleaching (FRAP) assays. The time-lapse experiments showed that the intracellular SYT1-GFP signal was highly dynamic, and different SYT1-GFP localizations within the transvacuolar strands were detected on frames separated by 15 s (Supplemental Movie S1). In contrast, the cortical SYT1-GFP signal was spatially restricted to largely stationary positions (Fig. 3A; Supplemental Fig. S5; Supplemental Movie S2). FRAP analysis of the cortical SYT1-GFP signals showed the recovery of 50% of the signal was achieved in less than 5 min (Fig. 3, B and C; Supplemental Movie S3). Notably, the recovered signal positions strongly resembled those marked by the prebleached SYT1-GFP, further supporting the nearly stationary nature of the SYT1-GFP cortical sites (Fig. 3D; Supplemental Fig. S5; Supplemental Movie S4).

The ER-PM Contact Sites Localize in Microtubule-Depleted Regions at the Cell Cortex

In actively dividing root epidermal cells, the SYT1 signal transitioned from the ER to the mitotic spindle at metaphase and was delivered to the forming cell plate during cytokinesis (Fig. 4A). This result suggests that the spatial localization of SYT1 might be partially controlled by the microtubule cytoskeleton. To further investigate this possible link, we performed colocalization studies of

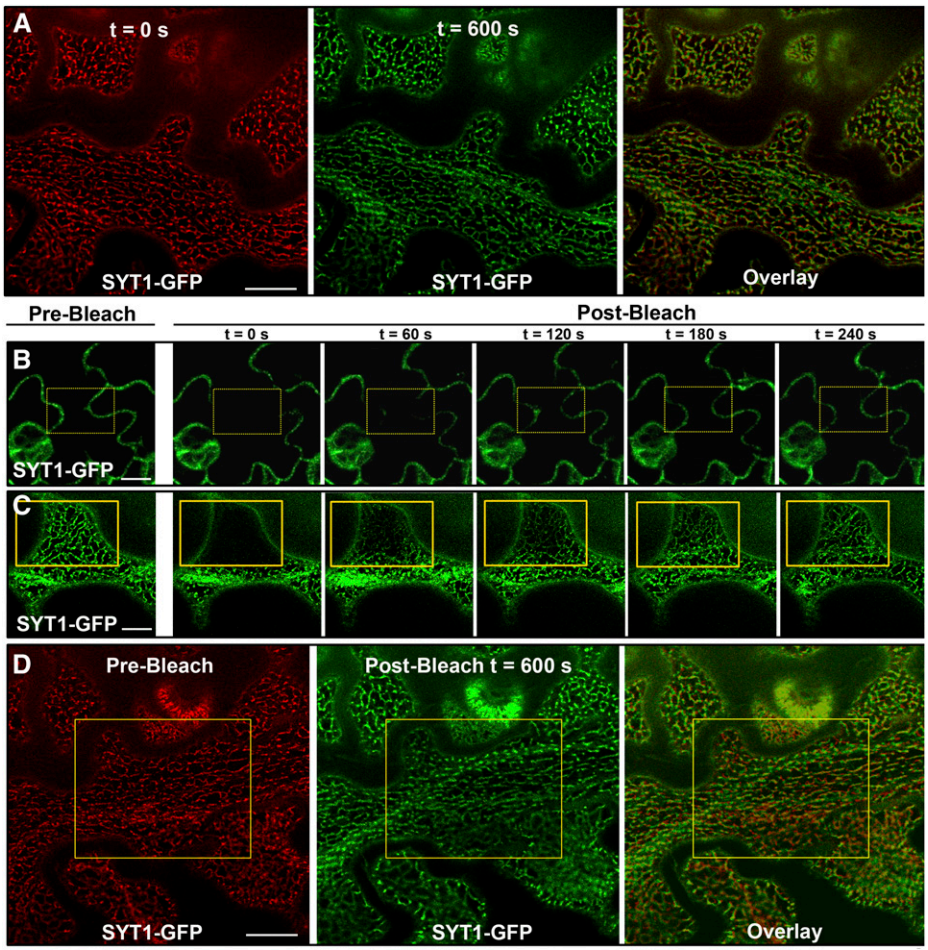

Figure 3. The SYT1-labeled ER-PM contact sites are predominantly stationary. A, SYT1-GFP signal comparison at the cortical regions of 8-d-old shoot epidermal cells during a 600-s time-lapse experiment. The initial (t = 0 s) and final (t = 600 s) frames are shown. Scale bars = 40 μm. B and C, Time course FRAP showing the recovery of the SYT1-GFP cortical signal at the equatorial plane (B) or cortical plane (C) in 8-d-old shoot epidermal cells. Scale bars = 40 μm. D, Pre- and post-FRAP SYT1-GFP signal comparison at the cortical regions of 8-d-old shoot epidermal cells. The initial (prebleach) and final (postbleach) frames of a representative 600-s FRAP experiment are shown. Scale bars = 40 μm.

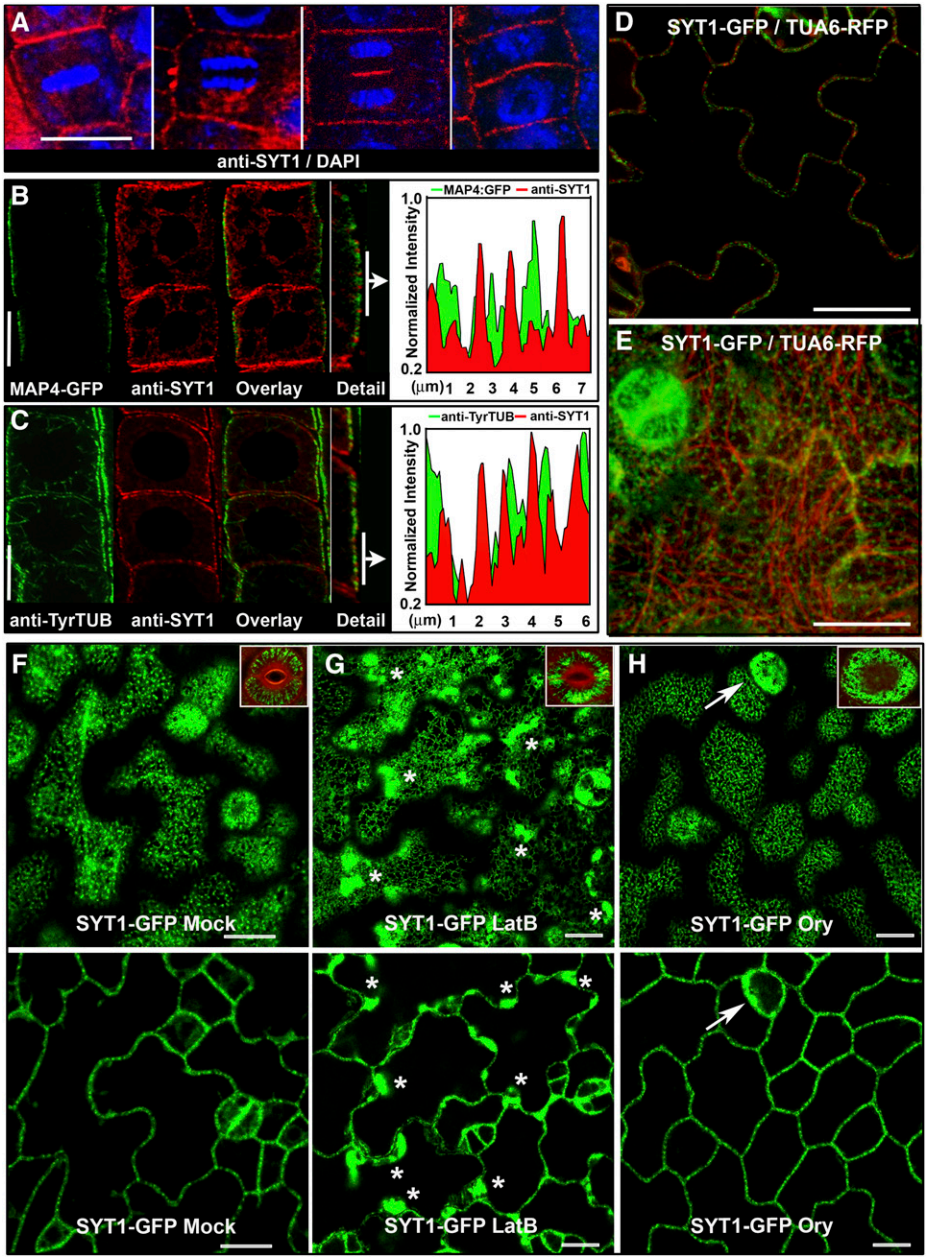

Figure 4. SYT1 is enriched in cortical cytoskeleton-depleted regions. A, SYT1 immunolocalization in dividing root epidermal cells. Different stages of cell division are indicated by 4′,6-diamino-phenylindole (DAPI) staining. B and C, Coimmunolocalization of SYT1 and the microtubule (MT) marker MAP4-GFP (B) or an anti-Tyr-tubulin IgG3 antibody (anti-TyrTUB; C). Intensity peaks for GFP (green) and tetramethylrhodamine (TRITC; red) were quantified using the pixel correlation function of the Leica LAS AF Lite platform. Scale bars = 10 μm. D and E, Colocalization analysis of the SYT1-GFP and TUA6-RFP markers in 4-d-old shoot epidermal cells from double transgenic lines: equatorial plane (D) and cortical plane (E). Scale bars = 50 μm. F to H, Effect of cytoskeleton-depolymerizing drugs in 4-d-old cotyledons harboring the SYT1-GFP construct. F, Twenty-four-hour control treatment using dimethyl sulfoxide. G, Twenty-four-hour treatment with the F-actin-depolymerizing drug latrunculin B (LatB; 1 μM). Asterisks mark intracellular SYT1-GFP aggregates. H, Twenty-four-hour treatment with the MT depolymerizing drug oryzalin (Ory; 25 μM). Arrow indicates the SYT1-GFP mislocalization in stomata. Scale bars = 20 μm. Insets show the effect of the drugs in guard cells.

SYT1 with different MT markers. In roots, the anti-SYT1 and the GFP-tagged mammalian MICROTUBULE-ASSOCIATED PROTEIN4 (MAP4-GFP) signals were mutually exclusive, indicating that the SYT1 puncta were mainly located within MT-depleted regions (Fig. 4B). The same result was obtained when the anti-SYT1 signal was compared with that generated by a monoclonal antibody that recognizes the tyrosinated form of the alpha-tubulin subunit (Fig. 4C). In shoots, we analyzed the SYT1 localization using a stable double transgenic line harboring the RFP-tagged TUBULIN6 (TUA6-RFP) and SYT1-GFP markers. As shown in Figure 4, D and E, both signals were largely separated with an estimated colocalization rate that ranged from 4% to 12%, depending on the sample and microscopy settings used (n = 24 cells). Finally, we treated lines expressing the Arabidopsis SYT1-GFP marker with cytoskeleton depolymerizing drugs. As shown in Figure 4, F to H (controls shown in Supplemental Fig. S6), F-actin depolymerization induced by latrunculin B abolished SYT1-GFP cytoplasmic streaming (Supplemental Movie S5) and caused the aggregation of the intracellular/ER SYT1-GFP pool, whereas the cortical pool remained mostly unaffected. Interestingly, oryzalin-mediated MT depolymerization changed neither the intracellular ER nor the cortical SYT1-GFP distributions in shoot epidermal cells, but changes in SYT1-GFP distributions were observed in mature guard cells (Fig. 4H). These

results suggest that, once established, the ER-PM contact sites do not require the cytoskeleton scaffold to maintain their position in leaf epidermal cells, but this process might be differentially regulated in guard cells.

The SYT1 C2 Domains Are Targeted to the PM and Bind Negatively Charged Phosphatidylinositol Phosphates

Similar to most tricalbins and E-Syts (Toulmay and Prinz, 2012; Giordano et al., 2013), SYT1 contains a predicted TM domain and phospholipid binding C2 domains through which it could connect the ER to the PM in trans. To assess the accuracy of these predictions and to distinguish between the two possible SYT1 orientations (TM anchored at the ER and C2 domains tethering the PM, or TM anchored at the PM and C2 domains tethering the ER), we first analyzed where isolated SYT1 C2 domains were targeted. For this purpose, we generated stable transgenic lines harboring the $SYT1_{244\text{-}541}$ peptide containing the GFP-tagged SYT1 C2 domains C2A and C2B (SYT1-C2AB; Schapire et al., 2008) fused to the 35S promoter. We also used a 35SproGFP and the SYT1-GFP lines as controls. As shown in Figure 5A, the 35SproGFP and the 35SproC2AB-GFP markers were both partially targeted to the nucleus, but whereas the 35SproGFP construct strongly labeled the cytosol, the 35SproC2AB-GFP construct was mainly targeted to the PM. This subcellular localization was further assessed by localization analysis of the different markers in plasmolyzed cells (Supplemental Fig. S7) and colocalization studies with the endocytic tracer *N*-(3-triethylammoniumpropyl)-4-{6-[4-(diethylamino) phenyl] hexatrienyl} pyridinium dibromide (FM4-64) that labels the PM in short-term treatments (Vida and Emr, 1995; Supplemental Fig. S8). In all cases, the subcellular localization of C2AB-GFP was different from the punctuated PM pattern observed for SYT1-GFP, suggesting that (1) the SYT1 TM domain is anchored to the ER and the C2 domains tether the PM, and (2) the SYT1 TM and SMP domains might restrict the positions where the SYT1 C2 domains bind to the PM; that is, to regions where the ER is in close contact with the PM.

In mammals, the E-Syts C2 domains have been reported to bind phosphatidylinositol phosphates (PtdInsPs) in both a Ca^{2+}-dependent and Ca^{2+}-independent manner (Giordano et al., 2013). Once we determined that the SYT1 C2 domains were targeted to the PM, we aimed to identify phospholipid species that might be involved in the C2-PM tethering process. Thus, we performed in vitro protein-lipid overlay assays using the purified SYT1-C2AB peptide in the presence or absence of Ca^{2+}. In the presence of Ca^{2+} (10 μM Ca^{2+}; Fig. 5B), the SYT1-C2AB peptide bound phosphatidylserine (PS), phosphatidic acid (PA), lysophosphatidic acid (LPA), and each of the negatively charged PtdInsPs, but not phosphatidylinositol (PtdIns). In the absence of Ca^{2+} (5 mM EGTA; Fig. 5B), the SYT1-C2AB strongly reduced the affinity for PS and slightly reduced the affinity for most of the PtdInsPs species. Together, these results suggest that the SYT1-C2AB binding to PM-localized PtdInsPs is largely Ca^{2+} independent and largely relies on electrostatic interactions.

SYT1 Confers Cellular Resistance to Mechanical Stress

Previous reports have shown that SYT1 loss of function causes hypersensitivity to conditions that

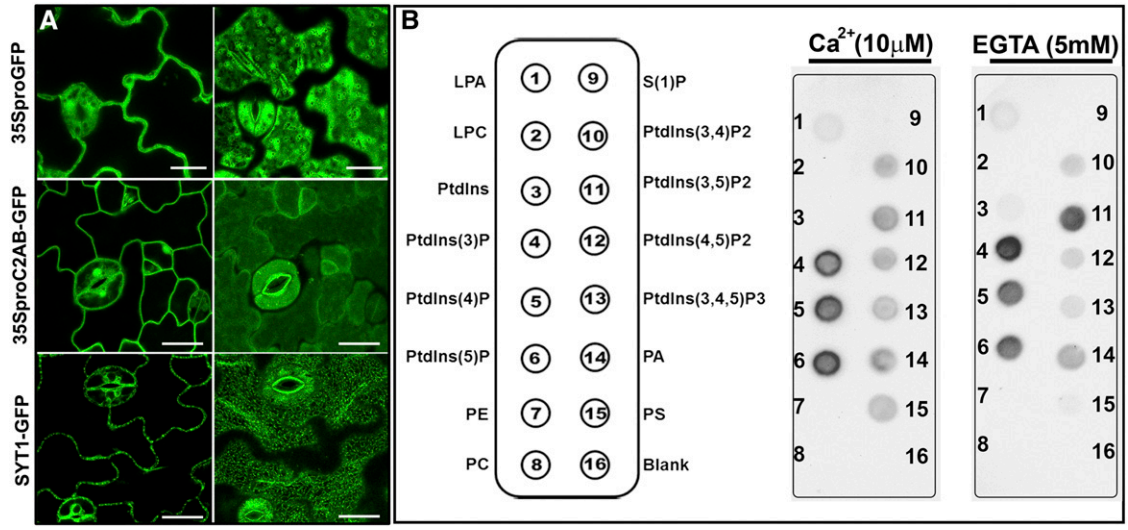

Figure 5. The SYT1 C2 domains are targeted to the PM and bind negatively charged PtdInsPs. A, Subcellular localization of the 35SproGFP, $35SproC2AB_{244\text{-}541}$-GFP, and SYT1-GFP markers in 5-d-old shoot epidermal cells. The equatorial (left) and cortical (right) planes are shown. Scale bars = 40 μm. B, Protein-lipid overlay assay. PIP Micro Strips (Life Technologies) were incubated with 0.5 μg mL^{-1} of the $SYT1_{244\text{-}541}$ C2AB soluble peptide in the presence (10 μM Ca^{2+}) or absence (5 mM EGTA) of Ca^{2+}. Binding was detected using the anti-SYT1 antibody. S(1)P, Sphingosine 1-phosphate; PE, phosphatidylethanolamine; PC, phosphatidylcholine.

generate changes in cellular turgor, such as osmotic, ionic, and freezing stresses (for review, see Schapire et al., 2009). Due to its subcellular localization and putative tethering function, we hypothesized that SYT1 might function as a structural component required to withstand external and internal physicomechanical forces. To gain further insights into this putative role, we determined whether the expression of *SYT1* responds to mechanical damage using transgenic plants transformed with the reporter β-glucuronidase gene driven by the SYT1 promoter (SYT1proGUS). As shown in Figure 6A, the SYT1proGUS signal was strongly induced by mechanical damage. Next, we analyzed the behavior of the SYT1-GFP marker subjected to controlled pressure (6,750 Pa). As shown in Figure 6B, the organized SYT1-GFP reticulated structures developed into more defined SYT1-GFP aggregates after 20-s treatments. A similar behavior was observed when the HDEL-GFP marker was used, suggesting that changes in ER morphology might represent an early response to mechanical stress. Under similar conditions, the cytoskeleton MAP4-GFP marker partially depolymerized, indicating that different cortical structures were quickly responding to mechanical stress cues (Fig. 6B). To investigate whether SYT1 has a functional role in mechanical stress responses, we next analyzed the cellular stability of the *syt1* mutant upon mechanical stress. First, we observed that *syt1* protoplasts displayed reduced tolerance to mechanical stress compared with the wild type, suggesting that SYT1 has a role in mechanical stress adaptation that is, at least in part, cell wall independent (Supplemental Fig. S9). In leaves, the application of mechanical stress inhibited their expansion and caused more extensive tissue damage in *syt1* compared with the wild type (Fig. 6C). The extent of the damage was further evaluated using trypan blue, a vital stain that cannot be excluded by dead cells. Although trypan blue stain was limited to a few individual cells within the pressed area in the wild type, the stain was observed in most cells either within or adjacent to the

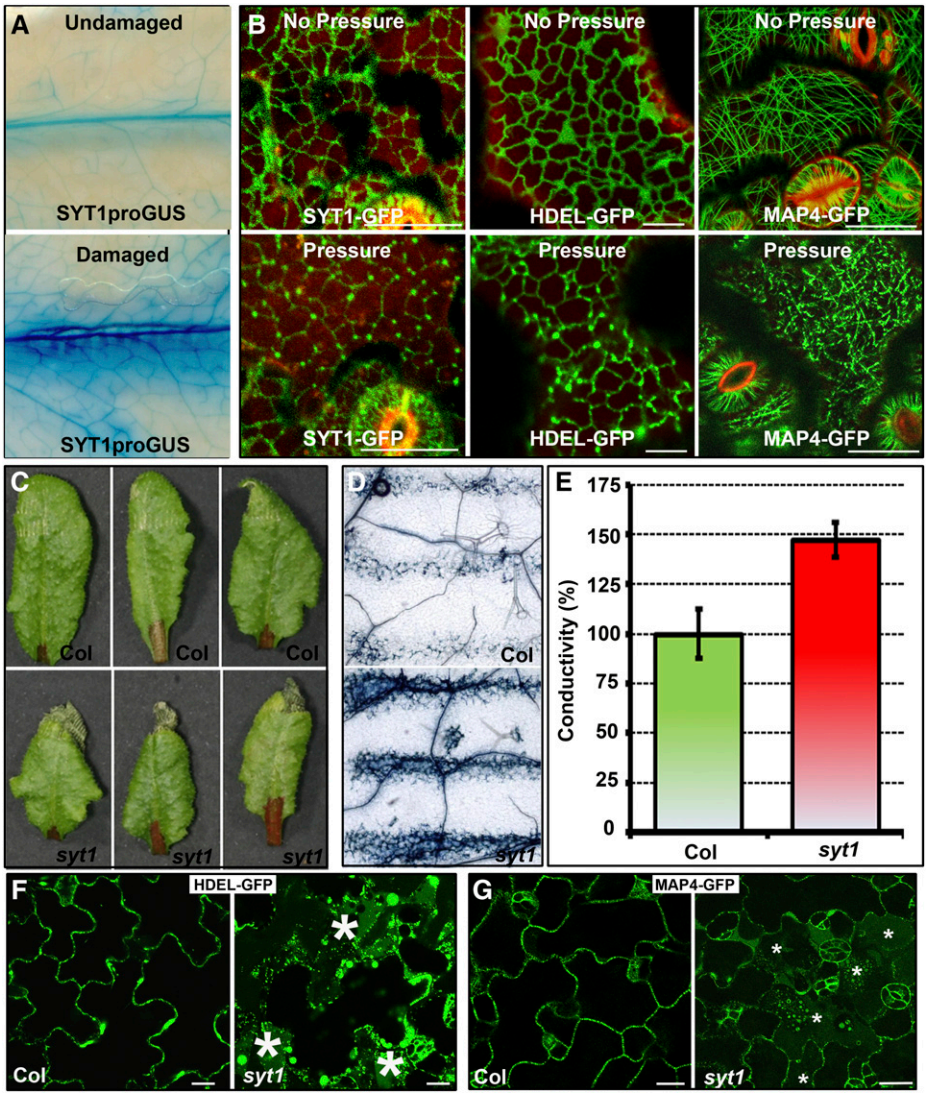

Figure 6. SYT1 confers tissue and cellular mechanotolerance. A, Histochemical GUS staining of control and mechanically damaged 3-week-old $SYT1_{pro}GUS$ plants. Plants were mechanically pressed with a 5-inch hemostate set to the first pressure level, and GUS staining was performed 1 h after the pressure treatment. B, Changes in the SYT1-GFP, HDEL-GFP, and MAP4-GFP localization upon mechanical stress load. Five-day-old seedlings were mounted on microscopy slides using water. Before imaging, a 330-g (6,750-Pa) weight was applied to the 22- × 22-mm coverslip for 20 s. Whereas the SYT1-GFP and HDEL-GFP markers form cortical aggregates when pressure approaches the cellular collapse limit, the MAP4-GFP marker shows MT depolymerization. Scale bars = 20 μm. C, Phenotype of mechanically wounded 6-week-old wild-type Columbia (Col) and *syt1* rosette leaves. Pictures were taken 3 d after wounding. D, Trypan blue staining of 6-week-old wild-type and *syt1* rosette leaves 1 h after wounding. E, Electrolyte leakage in 6-week-old wild-type and *syt1* leaf discs. Data are the means ± SD from three replicates ($n = 45$ leaf discs). Student's *t* test: $P \leq 0.01$. F and G, Cellular collapse of *syt1* epidermal cells upon mechanical load. Five-day-old Col and *syt1* harboring the HDEL-GFP and MAP4-GFP markers were loaded with a 330-g (6,750-Pa) weight and imaged after 20 s. Collapsed cells are marked with asterisks. Scale bars = 50 μm.

pressed area in *syt1* (Fig. 6D). This difference in damage was quantified by measuring electrolyte leakage of mechanically excised wild-type and *syt1* leaf discs. Figure 6E shows that the normalized conductivity of the solution containing *syt1* leaf discs was approximately 45% higher than that of the solution containing wild-type discs. Consistent with the observed mechanical stress hypersensitivity, the application of heavy mechanical loads (6,750 Pa) caused the collapse of 5% of the wild-type (n = 122) and 44% of the *syt1* (n = 120 cells) epidermal cells harboring the HDEL-GFP marker, and 3% of the wild-type (n = 103) and 28% of the *syt1* (n = 118 cells) epidermal cells harboring the MAP4-GFP marker (Fig. 6, F and G). Remarkably, the application of light mechanical loads (1,125 Pa) enhanced the depolymerization of the MAP4-GFP marker in *syt1* (74%; n = 131) compared with the wild type (14%; n = 107), indicating that this early mechanical response was also altered in the *syt1* background (Supplemental Fig. S10). Despite the multiple phenotypes associated with SYT1 depletion, no clear morphological differences at the cortical ER were observed between the wild type and *syt1* (Supplemental Fig. S11). This result suggests that SYT1 is important for ER-PM function, but additional components might be required for ER-PM contact sites establishment.

DISCUSSION

SYT1 Is a Plant ER-PM Phospholipid Binding Anchor

In yeast, three conserved protein families have been identified as ER-PM tethers: INCREASED SODIUM TOLERANCE2 (related to the mammalian anoctamin family of ion channels), the VAP proteins SUPPRESSOR OF CHOLINE SENSITIVITY2 (Scs2) and Scs22 and the tricalbin (Tcb) proteins Tcb1 to Tcb3 (orthologs of the extended synaptotagmin-like proteins E-Syt1 to E-Syt3 in mammals; Manford et al., 2012). Recently, a plant homolog of the yeast Scs2 protein, VAP27, was reported to localize at Arabidopsis ER-PM contact sites, identifying the first molecular components of such sites in plants (Wang et al., 2014). The Arabidopsis SYT1 contains the modular structure typical of tricalbins and E-Syts (Craxton, 2010; Yamazaki et al., 2010), is enriched at ER-PM subdomains, and similar to yeast, where Scs2 and Tcbs interact (Manford et al., 2012), it colocalizes with the ER-PM contact sites marker VAP27. Together, these results support the notion that an ER-PM tethering mechanism similar to that in yeast and mammals exists in plants.

To achieve their tethering function, most yeast tricalbins and mammalian E-Syts establish ER-PM contact sites in durable or transient states using a single amino-terminal ER anchor (Manford et al., 2012), the SMP domain that localizes them to specific ER-PM subdomains (Toulmay and Prinz, 2012), and a variable number of phospholipid binding domains (C2 domains) that connect the proteins to the PM in trans via electrostatic interactions with negatively charged phospholipids (Toulmay and Prinz, 2011; Manford et al., 2012; Giordano et al., 2013; Schauder et al., 2014). Our results suggest that the SYT1 localization at the nexus between the ER and the PM is restricted by its TM and SMP domains, and its docking to the PM mainly occurs through nonspecific electrostatic interaction with negatively charged PtdInsPs (Fig. 7A). These results highlight mechanistic similarities between the ER-PM contact sites establishment in plants and mammals, such as the Ca^{2+}-independent binding of phosphatidylinositol-4,5-bisphosphate observed in SYT1 and the mammalian E-Syt2 and E-Syt3 (Giordano et al., 2013). There are also

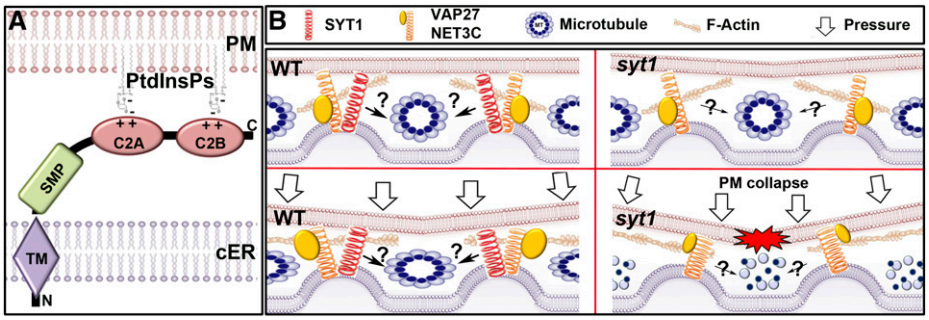

Figure 7. Putative roles of SYT1 in ER-PM contact sites. A, Docking mechanism: The SYT1 TM domain is anchored to the cortical ER (cER) and together with the SMP domain restricts the positions where the C2 domains dock to the PM. The C2 domains bind PM-localized PtdInsPs through largely Ca^{2+}-independent electrostatic interactions. B, SYT1 responses to mechanical stress. Top left, In a wild-type (WT) background, SYT1 is enriched in MT-depleted regions, colocalizes with ER-PM marker VAP27, and contributes to the PM stabilization by mechanically reinforcing the ER-PM contact sites. Top right, In an *syt1* background, SYT1 does not reinforce the ER-PM contact sites, but VAP27 and likely other ER-PM contact site components are sufficient to maintain the PM stability. Bottom left, In a mechanically challenged wild-type background, SYT1, the VAP27/NET3C complex, and the cortical MTs cooperate to distribute mechanical loads. Bottom right, In a mechanically challenged *syt1* background, the VAP27/NET3C complex and the cortical MTs are not sufficient to properly distribute mechanical loads; as a result, the cortical MTs depolymerize and the PM collapses. The mechanism (black arrows) by which the ER-PM contact sites might exchange information with cortical MTs remains unclear.

key differences between yeast and plant contact sites, such as the Ca^{2+}-dependent binding of PS observed in SYT1 that substitutes the Ca^{2+}-dependent binding of phosphatidylinositol-4,5-bisphosphate in the mammalian E-Syt1 (Giordano et al., 2013). Still, important mechanistic information, such as the putative presence of SYT1 in multiprotein tethering complexes involving VAP27/NET3C and other components, and the putative enrichment of ER-PM contact sites in specific phospholipids, is not yet defined in plants.

SYT1 Anchors the PM at MT-Depleted Regions

Similar to the Arabidopsis ER-PM contact site markers VAP27 and NET3C, the SYT1-GFP signal appears as a highly punctuated structure reminiscent of ER-PM anchor sites in both *N. benthamiana* and Arabidopsis epidermal cells (Wang et al., 2014). FRAP and time-lapse experiments showed that these structures were remarkably stationary, providing a clear distinction between the pools of highly dynamic intracellular SYT1 and stable cortical SYT1. Interestingly, a previous study has shown that VAP27 and NET3C associate tightly to the cortical MTs and F-actin cables, directly connecting the ER to the cortical cytoskeleton at ER-PM contact sites (Wang et al., 2014). Our data support and expand this view and suggest that the cortical tubulin cytoskeleton also provides positional cues for the establishment of ER-PM contact sites. In our model (Fig. 7B), the association of SYT1 puncta with the PM is largely restricted to MT-depleted regions in both roots and shoots, possibly because the tight associations between thick MTs (25 nm wide on average; Goddard et al., 1994) and the PM could pose steric impediments to the establishment of the narrow 10- to 30-nm (West et al., 2011) ER-PM contact sites. Remarkably, the organization of the putative SYT1-GFP anchors in cortical regions is mostly unaffected by the MT-depolymerizing drug oryzalin, suggesting that once established, the ER-PM contact sites do not require the cortical MT scaffold to maintain their fixed positions. Similar to the results observed for NET3C and VAP27 (Wang et al., 2014), latrunculin B abolished the SYT1-GFP movement through transvacuolar strands, indicating that the F-actin cables are important for the proper intracellular SYT1 turnover and transport. Taken all together, we propose two different roles for the plant cytoskeleton in ER-PM contact site formation: (1) The internal F-actin network functions as a carrier of SYT1 (and probably NET3C and VAP27) toward specific contact sites in different cell types; and (2) The cortical MT array provides positional information that allows the close apposition of ER and PM membranes for the establishment of ER-PM contact sites.

Putative Roles of SYT1 in Abiotic Stress Tolerance

Proper thigmostimuli perception is essential for plant growth and development, and two nonexclusive models of mechanoperception coexist in the plant literature. In the tensegrity model, mechanical deformations of the cell wall are finely modulated by the intrinsic instability of the MT cytoskeleton that senses the stress patterns. This process modifies the mechanical properties of plant cells through cellular endomembrane organization rearrangements (Brandizzi and Wasteneys, 2013) and targeted the deposition of rigidifying cell wall components (Landrein and Hamant, 2013; Sampathkumar et al., 2014). According to the tensegrity model, the SYT1-labeled ER-PM contact sites might function as deformable platforms that coordinate the cortical ER and cytoskeleton responses to minimize the mechanical loads at the PM. This model would not require the activation of transcriptional programs and can explain the instantaneous PM instability observed upon exposure to multiple stresses, including freezing, osmotic, and mechanical challenge (Yamazaki et al., 2008; Schapire et al., 2008; this study). This model could also explain the enhanced cytoskeleton depolymerization observed in the *syt1* mutant due to the limited ability of SYT1-depleted contact sites to properly transfer mechanical cues to the cortical cytoskeleton (Fig. 7B). An alternative tensegrity model for SYT1 is derived from mammalian cells where mechanical stimulation results in a reduced distance between the ER and the PM, thereby possibly enhancing transcompartment signaling and structural stabilization (Prinz, 2014). In this scenario, defects in transcompartment signaling could partially explain the general abiotic stress sensitivity observed in *syt1* that resembles the reduced survival under stress observed in mice lacking E-Syt2 and E-Syt3 tethers (Herdman et al., 2014).

Additionally, the ion-sensing model predicts that stress-inducible Ca^{2+}-dependent sensors decode mechanically triggered Ca^{2+} signatures (Kurusu et al., 2013). These putative sensors would transduce Ca^{2+} signatures by selectively binding to negatively charged phospholipids localized in the PM, such as the well-known PtdInsP signaling intermediates (Mosblech et al., 2008), or through direct interaction with putative stress-inducible Ca^{2+} binding partners (Hashimoto and Kudla, 2011). Our experimental results suggest that the SYT1 binding to PtdInsPs might be electrostatic and largely Ca^{2+} independent, which makes it an unlikely sensing mechanism; however, an intriguing possibility is that PS, and not PtdInsPs, might control downstream Ca^{2+}-dependent responses to mechanical stress in plants. At this point, we consider that the implications of the Ca^{2+}-dependent binding of PS during mechanical stress as well as the identification of putative stress-inducible and Ca^{2+}-dependent SYT1 binding partners are important aspects that need to be addressed by future research.

CONCLUSION

Our study identifies the Arabidopsis SYT1 as an essential component required for cellular resistance to mechanical stress acting as a putative ER-PM anchor. These

findings represent progress toward the understanding of ER-PM contact site functions in plant cells. Based on our results, we propose that the SYT1-labeled ER-PM contact sites represent conserved eukaryotic platforms where the close apposition between membranes coordinates the responses at the cell cortex and provides structural support against multiple environmental stresses. Future analysis of the SYT and VAP families of ER-PM markers represents a starting point for more precise elucidation of the role of plant ER-PM contact sites in the maintenance of PM stability upon stress exposure.

MATERIALS AND METHODS

Plant Growth and Chemical Treatments

For microscopy assays, surface-sterilized and cold-stratified Arabidopsis (*Arabidopsis thaliana*) seeds were grown as described in Rosado et al. (2012). For drug treatments, 4-d-old seedlings grown on solid one-half-strength Murashige and Skoog salts supplemented with 1% (w/v) Suc (basal medium) were transferred to 12-well plates containing liquid basal medium supplemented with 1 μM latrunculin B, 25 μM oryzalin, or mock (0.1% [v/v] dimethyl sulfoxide) and incubated for 24 h. After treatments, seedlings were rinsed and mounted on microscopy slides using water.

Cloning

The SYT1 and VAP27 constructs were generated through multisite gateway cloning. A 970-bp SYT1 promoter fragment (Benhamed et al., 2008) was cloned into pDONRP4P1R (Invitrogen), and a 615-bp UBQ10 promoter fragment was cloned in the pENTR 5′-TOPO vector. The genomic fragments of the SYT1 and VAP27 coding sequence were amplified from Col-0 DNA and recombined into pDONR221 (Invitrogen). The ER-targeted yellow cameleon 4.60 was subcloned from pBI121 vector (Iwano et al., 2009) into the multicloning site of pGEM3Zf(+) using restriction fragments generated by *Xba*I and *Sac*I, allowing for further subcloning into pENTR1A using the resulting *Sal*I and *Eco*RI restriction fragment. For the C-terminal XFP fusions (GFP, pEN-R2-F-L3,0; mRFP, pEN-R2-R-L3,0 [Karimi et al., 2007]; and TagRFP, pEN-R2-TagRFPSTOP-L3 [Mylle et al., 2013]), the respective entry vectors were recombined together with the respective promotor and coding sequence entry vectors into pKm43GW or pBm43GW (Karimi et al., 2005). For the promoter GUS construct, the SYT1 promoter fragment was recombined with pEN-L1-S-L2 into pKm42GW (Karimi et al., 2005). The obtained constructs were transformed into Col-0 via floral dip (Clough and Bent, 1998) or were used for transient expression in *Nicotiana benthamiana*.

Transient Expression in *N. benthamiana*

Suspensions of *Agrobacterium tumefaciens* strain LBA4404 harboring the different constructs were grown to an optical density at 600 nm of 0.5 and infiltrated into 4-week-old *N. benthamiana* leaves as previously described in Goodin et al. (2002). Transiently transformed leaves were imaged 3 to 5 d after infiltration using a Pascal Excite laser scanning confocal microscope (Zeiss) equipped with a 488-nm argon laser for GFP and a 543-nm He-Ne laser for RFP. Sequential line scanning mode was used to separate signals.

Immunostaining

Five-day-old root tips were used and all working solutions were prepared in microtubule stabilization buffer (50 mM PIPES, 5 mM EGTA, and 5 mM $MgSO_4$ [pH 7]). Sample preparation followed the basic protocol described in Sauer and Friml (2010). For immunodetection, a polyclonal rabbit anti-SYT1 antibody (1:1,000) or a monoclonal anti-Tyr-tubulin mouse IgG3 (TUB-1A2; Sigma-Aldrich; 1:400) was incubated overnight at 4°C. For immunodetection, the root tips were incubated for 1 h with TRITC-conjugated AffiniPure Donkey anti-Rabbit IgG (1:200; Jackson Immunoresearch), Alexa Fluor 488 Goat anti-mouse (1:600; Invitrogen) and/or sheep anti-rabbit IgG (whole molecule), F(ab′)2 fragment-Cy3 (1:600; Sigma-Aldrich), and mounted on microscopy slides using the glycerol-based AF1 Mountant Solution (Citifluor).

Immunogold TEM

Five-day-old roots were high-pressure frozen using a Leica HPM 100 with B-type sample carriers with 1-hexadecene as a cryoprotectant. Cryofixed samples were freeze substituted in 0.25% glutaraldehyde, 0.1% uranyl acetate, and 8% dimethoxypropane in acetone, embedded in LR white resin (London Resin Company Ltd), sectioned, and poststained as described (McFarlane et al., 2008). Immunolabeling was performed according to McFarlane et al. (2008) with 1:100 primary anti-SYT1 antibody and 1:100 goat-anti-rabbit 10-nm gold conjugate (BBI Solutions). As negative controls, wild-type sections were treated without primary antibody, and *syt1* mutant sections were treated with anti-SYT1 and the gold-conjugated secondary antibody. Samples were imaged at 0.8 kV using a Zeiss EM910 coupled to an Olympus Quemesa CCD camera.

Confocal Imaging

Immunolocalization and cell viability images were obtained using a Leica TCS SP5 II or a Zeiss 710 confocal microscope equipped with 405-nm diode lasers for 4′,6-diamino-phenylindole, a 488-nm argon laser for GFP, Alexa488 and fluorescein diacetate, and a 561-nm He-Ne laser for FM4-64, Cy3, and TRITC signals. For colocalization and cellular integrity analyses, sequential line scanning mode was used to separate signals. The SYT1-GFP images were obtained using a Zeiss-Pascal Excite laser scanning confocal microscope equipped with a 488-nm argon laser for GFP and a 543-nm He-Ne Laser for propidium iodide. For FRAP analysis, we adjusted the laser intensity and performed a single bleaching scan using a 405-nm diode laser. We collected images before and after bleaching using low laser intensities and monitored FRAP for 15 min with data acquisition points every 20 s. All microscopy images were processed using the Leica LAS AF Lite platform or the Java-based image processing program ImageJ (National Institutes of Health). All article figures were assembled using Adobe Photoshop CS.

Protein Lipid Overlay Assay

The phospholipid-binding analysis of the $SYT1_{244\text{-}541}$ C2AB peptide was conducted using PIP Strips (Molecular Probes) as described by the manufacturer. In brief, the PIP strips were blocked for 1 h in 3% bovine serum albumin in Tris-buffered saline plus Tween 20 supplemented with either 10 μM $CaCl_2$ or 5 mM EGTA and then incubated overnight at 4°C in blocking buffer containing 0.5 μg mL^{-1} $SYT1_{244\text{-}541}$ C2AB peptide. The strips were incubated with the primary anti-SYT1 antibody (1:1,000) for 2 h and with the secondary horseradish peroxidase-conjugated goat anti-rabbit antibody (IgG-HRP, Santa Cruz Biotechnology, 1:14,000) for 1 h. The chemiluminiscent signal was detected using the Clarity western enhanced chemiluminescence substrate (Bio-Rad).

Mechanical Treatments

Fully expanded 6-week-old rosette leaves from plants grown under short-day photoperiod (8 h of light/16 h of dark) were mechanically pressed perpendicularly to the midrib using the first pressure level of a surgical hemostatic clamp. After 1-h treatment, leaves were harvested and incubated for 6 min in boiling trypan blue staining solution (trypan-blue stock solution [10 g of phenol, 10 mL of lactic acid, 10 mL of glycerol, 10 mg of trypan blue] diluted 1:1 with ethanol) and changed to chloral hydrate destaining solution (2.5 g mL^{-1} in water). The destaining solution was changed several times during the next 3-d period, and the destained leaves were mounted on microscopy slides using 50% glycerol. Images were acquired using a Nikon Eclipse E 800 differential interference contrast microscope. For mechanical treatments at the cellular level, 5-d-old seedlings were mounted on microscopy slides using water, and variable weights ranging from 50 to 350 g were applied to the 22- × 22-mm coverslip for 20 s. Pressed cotyledons were observed under a confocal microscope immediately after treatment.

Sequence data from this article can be found in the GenBank/EMBL data libraries under accession number At2g20990 for SYT1. The *syt1-2* allele used in the study corresponds to the transfer DNA insertion line SAIL_775_A08 (Arabidopsis Biological Resource Center stock no. CS834629).

Supplemental Data

The following supplemental materials are available.

Supplemental Figure S1. Functional domains of SYT orthologs and anti-SYT1 antibody specificity.

Supplemental Figure S2. SYT1 colocalization with different PM markers.

Supplemental Figure S3. Comparison between SYT1 and different ER markers.

Supplemental Figure S4. ImmunoTEM controls.

Supplemental Figure S5. SYT1-GFP time lapse and FRAP experiments.

Supplemental Figure S6. Chemical treatment controls.

Supplemental Figure S7. Subcellular localization of the 35SproGFP, 35SproC2AB, and SYT1-GFP markers in plasmolyzed cells.

Supplemental Figure S8. Colocalization of the 35SproGFP, 35SproC2AB, and SYT1-GFP markers with FM4-64.

Supplemental Figure S9. Protoplast viability assay in wild-type and *syt1* backgrounds.

Supplemental Figure S10. Severing activity upon mechanical stress in wild-type and *syt1* backgrounds.

Supplemental Figure S11. Gross ER morphology in wild-type and *syt1* backgrounds.

Supplemental Movie S1. SYT1-GFP marker movement through transvacuolar strands.

Supplemental Movie S2. Time-lapse experiment using the SYT1-GFP marker.

Supplemental Movie S3. FRAP analysis using the SYT1-GFP marker.

Supplemental Movie S4. FRAP analysis of the SYT1-GFP cortical signal.

Supplemental Movie S5. SYT1-GFP signal upon treatment with LatB.

ACKNOWLEDGMENTS

We thank Dr. Natasha Raikhel (University of California, Riverside) and the Samuel's laboratory (University of British Columbia, Vancouver) for research discussions; Luke Busta (University of British Columbia, Vancouver) for critical reading of the article; Dr. Stéphanie Robert (Umeå Plant Science Center) and Dr. Geoffrey Wasteneys (University of British Columbia, Vancouver) for the HDEL-GFP, SECRETORY 12P-LIKE-GFP, MAP4-GFP, and GFP-TUA6 marker lines; Dr. Arnaldo L. Schapire (University of Malaga) and Dr. Teagen Quilichini, Jayme Kim, Morvarid Mehrtash, and Joseliya Embuscado (University of British Columbia, Vancouver) for technical assistance.

Received February 18, 2015; accepted March 17, 2015; published March 19, 2015.

LITERATURE CITED

Almeras T, Costes E, Salles JC (2004) Identification of biomechanical factors involved in stem shape variability between apricot tree varieties. Ann Bot (Lond) **93:** 455–468

Arnadóttir J, Chalfie M (2010) Eukaryotic mechanosensitive channels. Annu Rev Biophys **39:** 111–137

Benhamed M, Martin-Magniette ML, Taconnat L, Bitton F, Servet C, De Clercq R, De Meyer B, Buysschaert C, Rombauts S, Villarroel R, et al (2008) Genome-scale Arabidopsis promoter array identifies targets of the histone acetyltransferase GCN5. Plant J **56:** 493–504

Berghöfer T, Eing C, Flickinger B, Hohenberger P, Wegner LH, Frey W, Nick P (2009) Nanosecond electric pulses trigger actin responses in plant cells. Biochem Biophys Res Commun **387:** 590–595

Brandizzi F, Wasteneys GO (2013) Cytoskeleton-dependent endomembrane organization in plant cells: an emerging role for microtubules. Plant J **75:** 339–349

Carr CM, Munson M (2007) Tag team action at the synapse. EMBO Rep **8:** 834–838

Clough SJ, Bent AF (1998) Floral dip: a simplified method for *Agrobacterium*-mediated transformation of *Arabidopsis thaliana*. Plant J **16:** 735–743

Craxton M (2010) A manual collection of Syt, Esyt, Rph3a, Rph3al, Doc2, and Dblc2 genes from 46 metazoan genomes—an open access resource for neuroscience and evolutionary biology. BMC Genomics **11:** 37

Fuller RB (1961) Tensegrity. Portfolio and Art News Annual **4:** 112–127

Giordano F, Saheki Y, Idevall-Hagren O, Colombo SF, Pirruccello M, Milosevic I, Gracheva EO, Bagriantsev SN, Borgese N, De Camilli P (2013) PI(4,5)P(2)-dependent and Ca(2+)-regulated ER-PM interactions mediated by the extended synaptotagmins. Cell **153:** 1494–1509

Goddard RH, Wick SM, Silflow CD, Snustad DP (1994) Microtubule components of the plant cell cytoskeleton. Plant Physiol **104:** 1–6

Goodin MM, Dietzgen RG, Schichnes D, Ruzin S, Jackson AO (2002) pGD vectors: versatile tools for the expression of green and red fluorescent protein fusions in agroinfiltrated plant leaves. Plant J **31:** 375–383

Hashimoto K, Kudla J (2011) Calcium decoding mechanisms in plants. Biochimie **93:** 2054–2059

Helle SC, Kanfer G, Kolar K, Lang A, Michel AH, Kornmann B (2013) Organization and function of membrane contact sites. Biochim Biophys Acta **1833:** 2526–2541

Herdman C, Tremblay MG, Mishra PK, Moss T (2014) Loss of Extended Synaptotagmins ESyt2 and ESyt3 does not affect mouse development or viability, but in vitro cell migration and survival under stress are affected. Cell Cycle **13:** 2616–2625

Ingber DE (2008) Tensegrity-based mechanosensing from macro to micro. Prog Biophys Mol Biol **97:** 163–179

Iwano M, Entani T, Shiba H, Kakita M, Nagai T, Mizuno H, Miyawaki A, Shoji T, Kubo K, Isogai A, et al. (2009) Fine-tuning of the cytoplasmic Ca^{2+} concentration is essential for pollen tube growth. Plant Physiol **150:** 1322–1334

Jensen GS, Haswell ES (2012) Functional analysis of conserved motifs in the mechanosensitive channel homolog MscS-Like2 from Arabidopsis thaliana. PLoS ONE **7:** e40336

Karimi M, De Meyer B, Hilson P (2005) Modular cloning in plant cells. Trends Plant Sci **10:** 103–105

Karimi M, Depicker A, Hilson P (2007) Recombinational cloning with plant gateway vectors. Plant Physiol **145:** 1144–1154

Komis G, Apostolakos P, Galatis B (2002) Hyperosmotic stress induces formation of tubulin macrotubules in root-tip cells of Triticum turgidum: their probable involvement in protoplast volume control. Plant Cell Physiol **43:** 911–922

Kurusu T, Kuchitsu K, Nakano M, Nakayama Y, Iida H (2013) Plant mechanosensing and Ca^{2+} transport. Trends Plant Sci **18:** 227–233

Landrein B, Hamant O (2013) How mechanical stress controls microtubule behavior and morphogenesis in plants: history, experiments and revisited theories. Plant J **75:** 324–338

Lewis JD, Lazarowitz SG (2010) Arabidopsis synaptotagmin SYTA regulates endocytosis and virus movement protein cell-to-cell transport. Proc Natl Acad Sci USA **107:** 2491–2496

Manford AG, Stefan CJ, Yuan HL, Macgurn JA, Emr SD (2012) ER-to-plasma membrane tethering proteins regulate cell signaling and ER morphology. Dev Cell **23:** 1129–1140

McFarlane HE, Young RE, Wasteneys GO, Samuels AL (2008) Cortical microtubules mark the mucilage secretion domain of the plasma membrane in Arabidopsis seed coat cells. Planta **227:** 1363–1375

Mirabet V, Das P, Boudaoud A, Hamant O (2011) The role of mechanical forces in plant morphogenesis. Annu Rev Plant Biol **62:** 365–385

Monshausen GB, Haswell ES (2013) A force of nature: molecular mechanisms of mechanoperception in plants. J Exp Bot **64:** 4663–4680

Mosblech A, König S, Stenzel I, Grzeganek P, Feussner I, Heilmann I (2008) Phosphoinositide and inositolpolyphosphate signalling in defense responses of Arabidopsis thaliana challenged by mechanical wounding. Mol Plant **1:** 249–261

Mylle E, Codreanu MC, Boruc J, Russinova E (2013) Emission spectra profiling of fluorescent proteins in living plant cells. Plant Methods **9:** 10

Nick P (2013) Microtubules, signalling and abiotic stress. Plant J **75:** 309–323

Prinz WA (2014) Bridging the gap: membrane contact sites in signaling, metabolism, and organelle dynamics. J Cell Biol **205:** 759–769 10.1083/jcb.201401126

Rosado A, Li R, van de Ven W, Hsu E, Raikhel NV (2012) Arabidopsis ribosomal proteins control developmental programs through translational regulation of auxin response factors. Proc Natl Acad Sci USA **109:** 19537–19544

Sampathkumar A, Krupinski P, Wightman R, Milani P, Berquand A, Boudaoud A, Hamant O, Jönsson H, Meyerowitz EM (2014) Subcellular and supracellular mechanical stress prescribes cytoskeleton behavior in Arabidopsis cotyledon pavement cells. eLife **3:** e01967

Sauer M, Friml J (2010) Immunolocalization of proteins in plants. Methods Mol Biol **655:** 253–263

Schapire AL, Valpuesta V, Botella MA (2009) Plasma membrane repair in plants. Trends Plant Sci **14:** 645–652

Schapire AL, Voigt B, Jasik J, Rosado A, Lopez-Cobollo R, Menzel D, Salinas J, Mancuso S, Valpuesta V, Baluska F, et al. (2008) Arabidopsis synaptotagmin 1 is required for the maintenance of plasma membrane integrity and cell viability. Plant Cell **20:** 3374–3388

Schauder CM, Wu X, Saheki Y, Narayanaswamy P, Torta F, Wenk MR, De Camilli P, Reinisch KM (2014) Structure of a lipid-bound extended synaptotagmin indicates a role in lipid transfer. Nature **510:** 552–555

Staehelin LA (1997) The plant ER: a dynamic organelle composed of a large number of discrete functional domains. Plant J **11:** 1151–1165

Sukharev S, Sachs F (2012) Molecular force transduction by ion channels: diversity and unifying principles. J Cell Sci **125:** 3075–3083

Telewski FW (2006) A unified hypothesis of mechanoperception in plants. Am J Bot **93:** 1466–1476

Toulmay A, Prinz WA (2011) Lipid transfer and signaling at organelle contact sites: the tip of the iceberg. Curr Opin Cell Biol **23:** 458–463

Toulmay A, Prinz WA (2012) A conserved membrane-binding domain targets proteins to organelle contact sites. J Cell Sci **125:** 49–58

Vida TA, Emr SD (1995) A new vital stain for visualizing vacuolar membrane dynamics and endocytosis in yeast. J Cell Biol **128:** 779–792

Wang P, Hawkins TJ, Richardson C, Cummins I, Deeks MJ, Sparkes I, Hawes C, Hussey PJ (2014) The plant cytoskeleton, NET3C, and VAP27 mediate the link between the plasma membrane and endoplasmic reticulum. Curr Biol **24:** 1397–1405

West M, Zurek N, Hoenger A, Voeltz GK (2011) A 3D analysis of yeast ER structure reveals how ER domains are organized by membrane curvature. J Cell Biol **193:** 333–346

Yamazaki T, Kawamura Y, Minami A, Uemura M (2008) Calcium-dependent freezing tolerance in *Arabidopsis* involves membrane resealing via synaptotagmin SYT1. Plant Cell **20:** 3389–3404

Yamazaki T, Takata N, Uemura M, Kawamura Y (2010) Arabidopsis synaptotagmin SYT1, a type I signal-anchor protein, requires tandem C2 domains for delivery to the plasma membrane. J Biol Chem **285:** 23165–23176

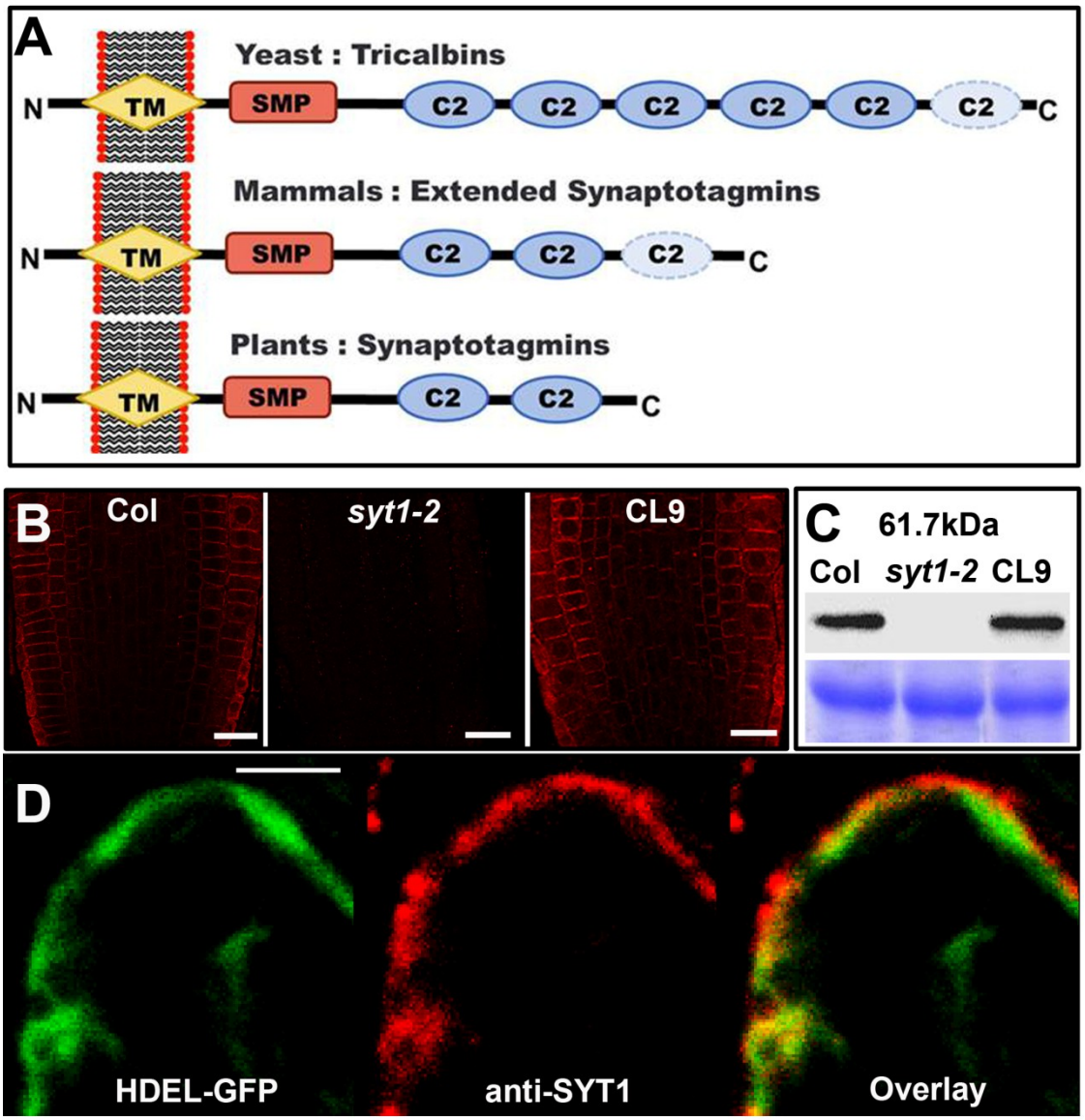

Figure S1. A) Schematic representation of the functional domains of the yeast Tricalbins, mammalian Extended Synaptotagmins and plant synaptotagmin, dashed C2 domains might not be present in all family members. **B)** Specificity of the rabbit AntiSYT1$_{244\text{-}541}$. SYT1 immunolocalization in wild-type (Col), *syt1-2* mutant allele (*syt1*) and the *syt1* complemented line CL9 (Schapire et al., 2008). Scale bars = 50µm. **C)** Western blot of the lines described in B shows a specific SYT1 signal at approximately 61kDa that closely resemble the predicted 61.7 kDa mass of the SYT1 protein. Coomassie blue staining was used to ensure equal loading. **D)** Detail of the cortical region of a 5-day-old root epidermal cell displaying the close apposition of the HDEL-GFP and anti-SYT1 signals. Scale bar 4µm.

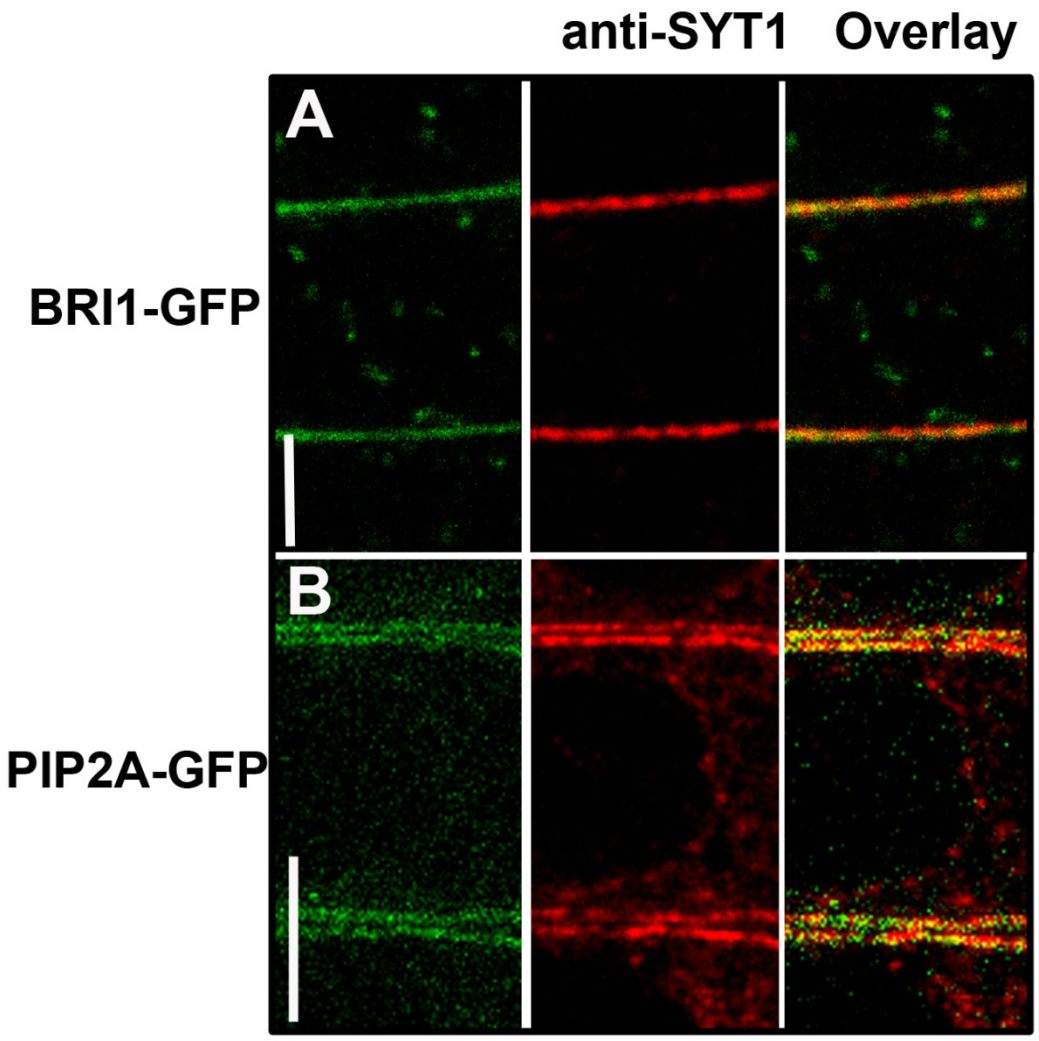

Figure S2. SYT1 co-localizes with PM markers in root epidermal cells. (A-B) Co-immunolocalization of the endogenous SYT1 signal with the plasma membrane BRI1-GFP **(A)** and PIP2A-GFP **(B)** markers in 5-day-old root epidermal cells. Scale bar = 10µm.

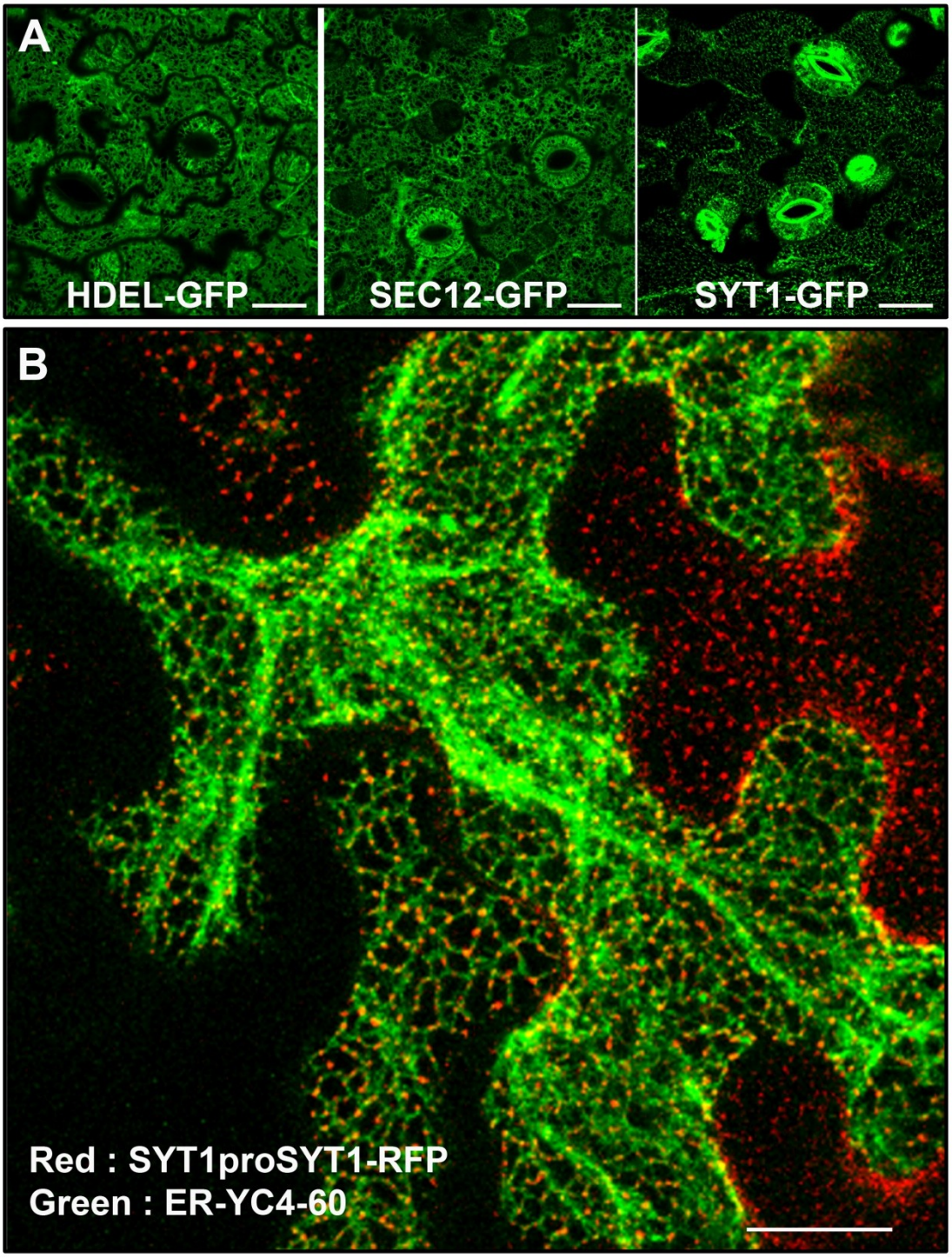

Figure S3. A) Comparison of the signal patterns of the luminal ER marker HDEL-GFP (Bolte et al., 2004), the ER membrane marker SEC12-GFP (da Silva et al., 2004) and SYT1-GFP. Images were acquired in the cortical region of 8-day-old leaf epidermal cells. Scale bar = 30µm. **B)** Transient co-localization of the SYT1proSYT1-RFP and ER-targeted YC4.6 markers in *N. benthamiana* epidermal cells. The SYT1proSYT1-RFP signal shows a punctate pattern that co-localizes with the ER marker. Scale bar = 50µm.

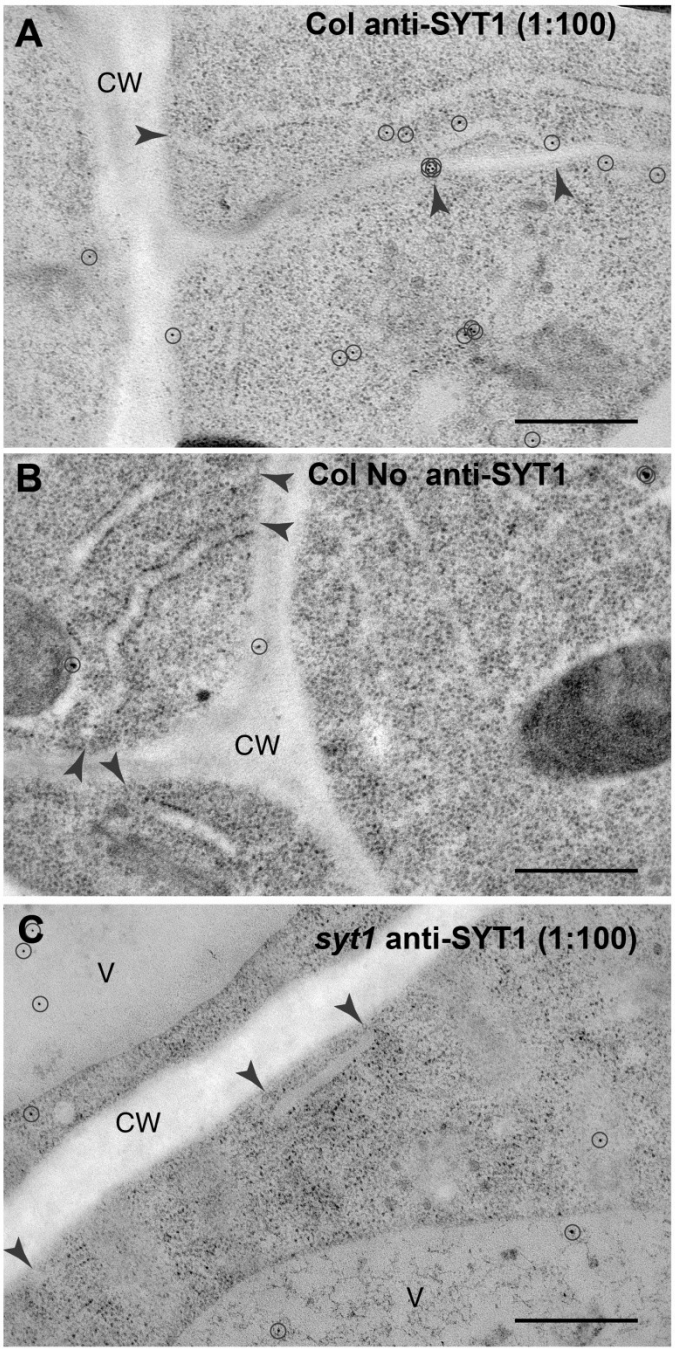

Figure S4. (A-C) ImmunoTEM of high-pressure frozen, freeze substituted wild type and *syt1* roots probed with anti-SYT1 and a 10nm gold-conjugated secondary antibody. Background was detected in the cell wall, cytoplasm, nucleus, and other organelles in wild type and this background signal was also detected in *syt1* mutants probed with the same antibodies. No significant cortical ER labeling was detected in the mutants probed with anti-SYT1. Circles highlight gold particles, CW = cell wall, V = vacuole, arrow heads point to ER-PM contact sites. Scale bars =500nm.

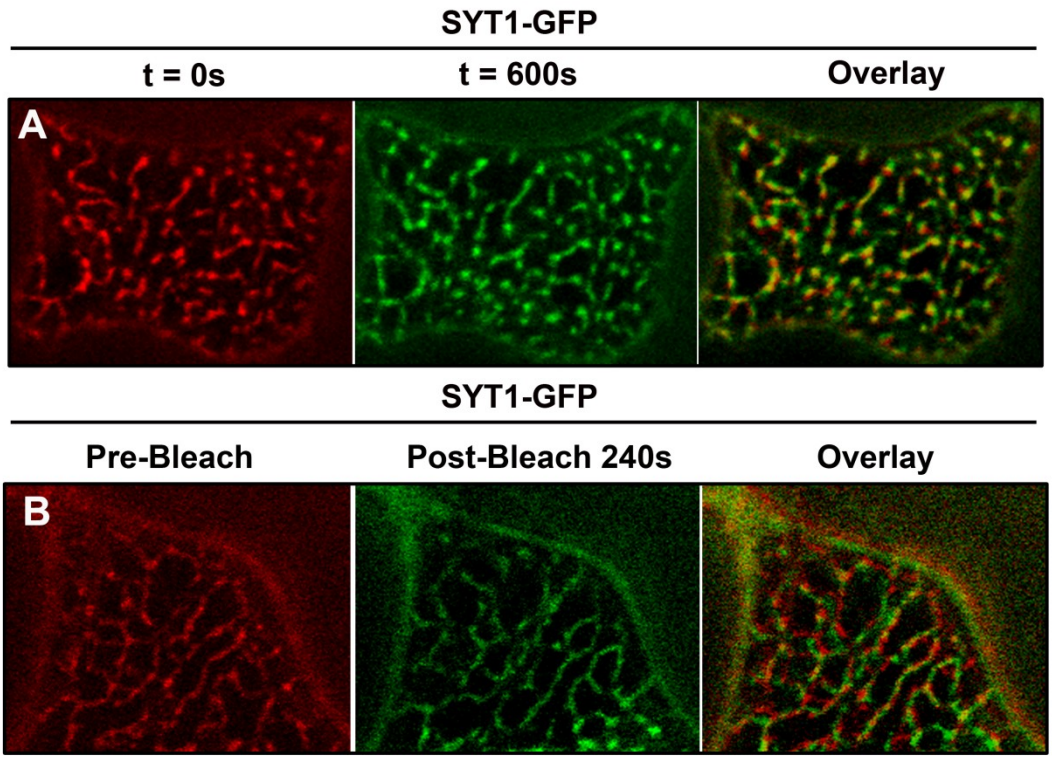

Figure S5. A) Time lapse experiment (Detail). SYT1-GFP signal comparison at the cortical regions of 8-day-old shoot epidermal cells during a 600 s time lapse experiment. The initial (t= 0s) and final (t = 600 s) frames are shown. **B) FRAP experiment (Detail)** Pre- and Post-FRAP SYT1-GFP signal comparison at the cortical regions of 8-day-old shoot epidermal cells. The initial (Pre-bleach) and final (Post-bleach) frames of a representative 240 s FRAP experiment is shown.

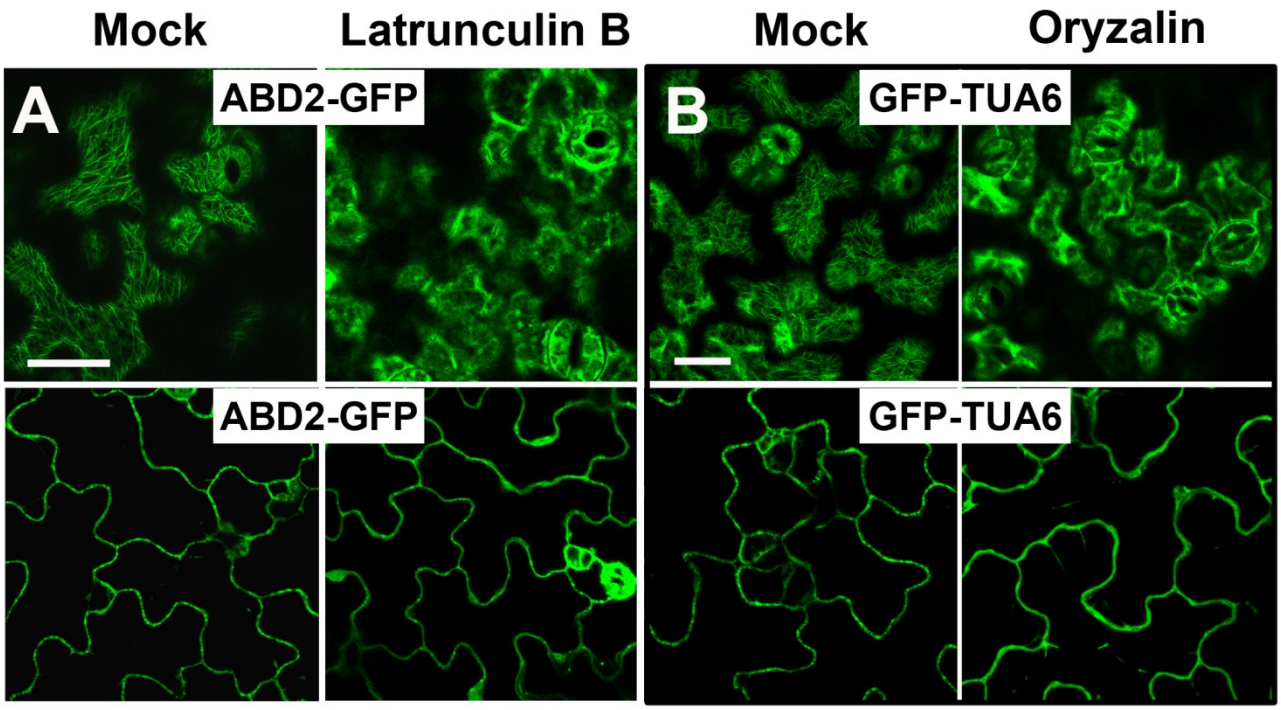

Figure S6. Chemical treatment controls A) The Actin marker ABD2-GFP was used as a positive control of depolymerization for the Latrunculin B treatment. **B)** The tubulin marker GFP-TUA6 was used as a positive control of depolymerization for the Oryzalin treatment. Upper panel cortical plane, Bottom panels: Equatorial plane. Scale bars = 50µm.

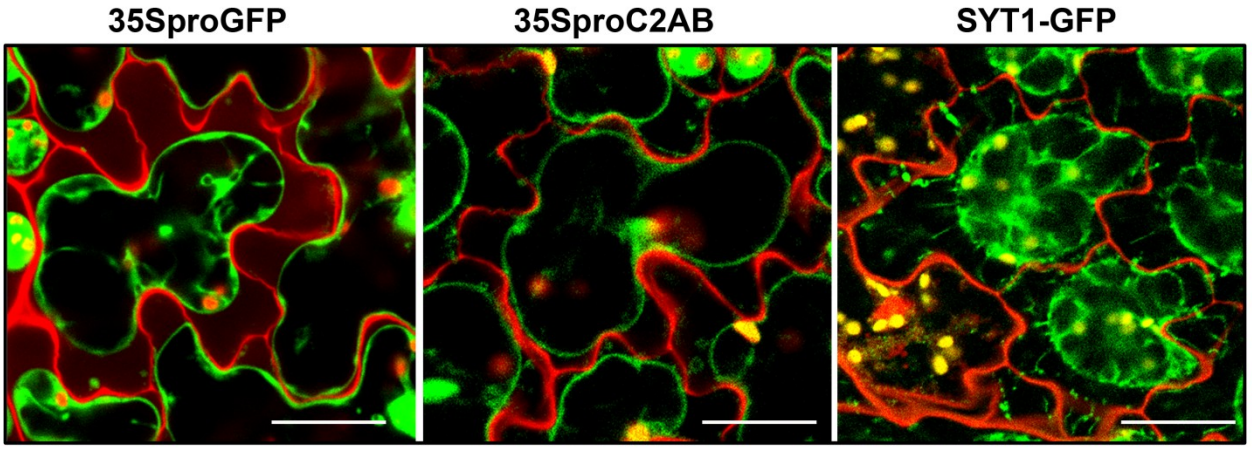

Figure S7. Subcellular localization of the 35SproGFP, 35SproC2AB and SYT1-GFP markers in plasmolyzed shoot epidermal cells. Plasmolysis was achieved by 5 minutes treatments with a 0.8M Mannitol solution. Scale bar = 40μm.

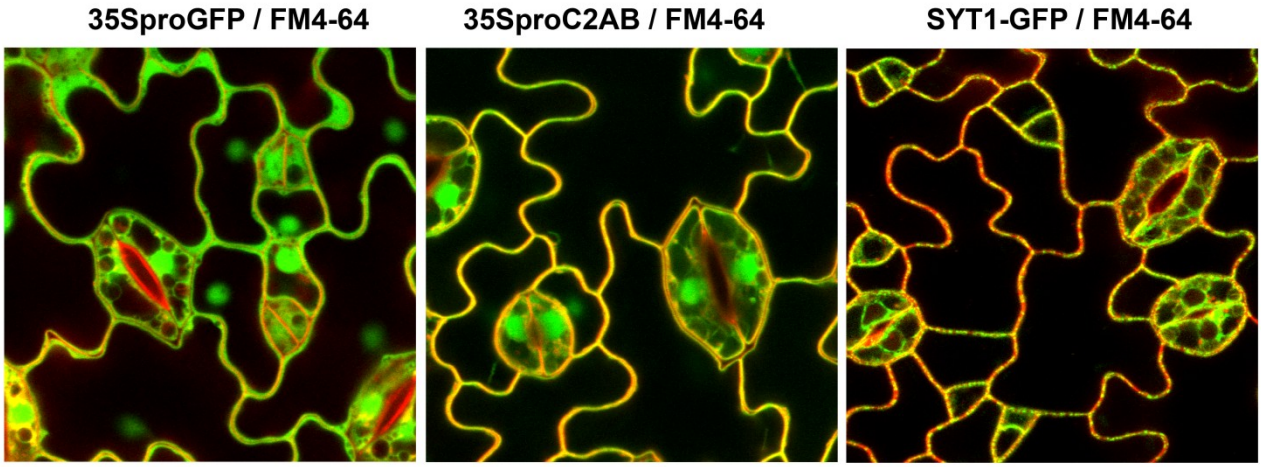

Figure S8. Co-localization of the 35SproGFP, 35SproC2AB and SYT1-GFP markers with the endocytic dye FM4-64 in 8-day-old shoot epidermal cells. Images were taken after incubation with 10 μM FM4-64 for 2 minutes.

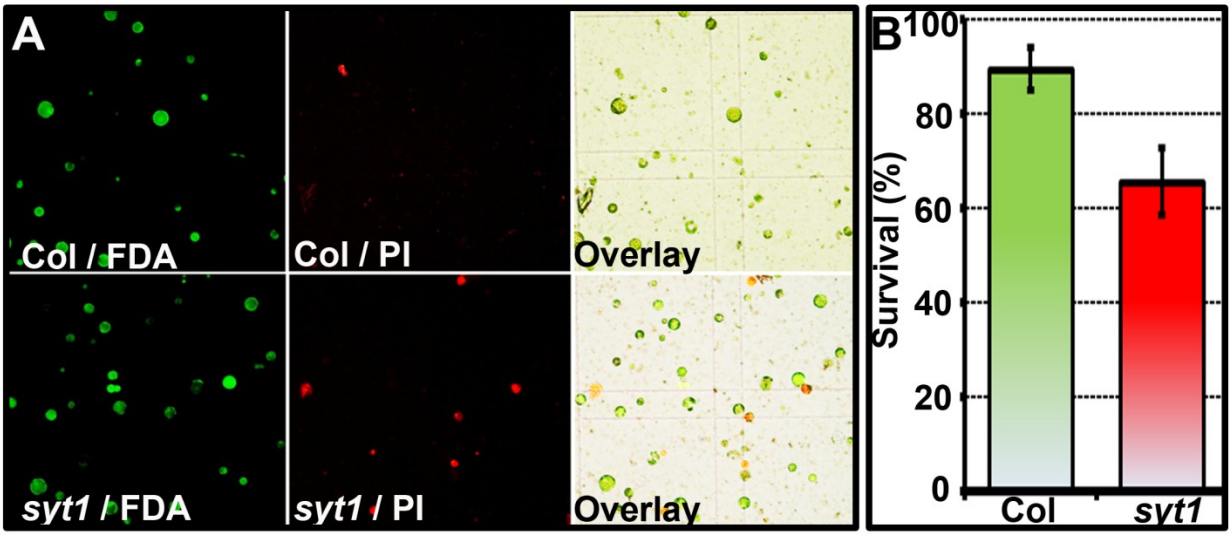

Figure S9. Protoplast viability assay. Protoplasts were isolated using the Tape-Arabidopsis Sandwich (Wu et al., 2009) and an aliquot was incubated with 10µM FM464 and 5µg/ml FDA for 5min and placed in a Neubauer counting grid for quantification. A similar procedure was performed after the 100 x g centrifugation treatments. Protoplast survival was estimated *as* a fraction of fluorescein diacetate (FDA = alive) / Propidium Iodide (PI = dead) stained cells. Results were represented after normalization with their respective controls. Data are the means ± standard deviation of three independent experiments n=400 Student's t-test P= < 0.005.

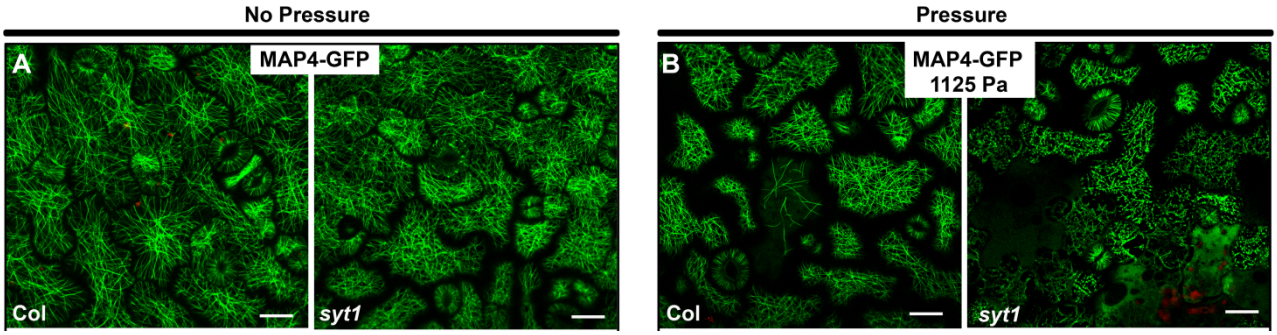

Figure S10. *syt1* displays enhanced microtubule severing upon mechanical stress. Five-day-old WT and *syt1* seedlings harboring the MAP4-GFP markers were grown in the same plate and mounted on microscopy slides using water. **(A)** Pictures of WT and *syt1* harboring MAP4-GFP in non-stressed conditions. **(B)** Pictures of WT and *syt1* harboring MAP4-GFP after a 20s mechanical load applications of 55 g (1125 Pa). Increased severing activity is shown as shorter cortical microtubules in the *syt1* MAP4-GFP background. Scale bar = 20µm.

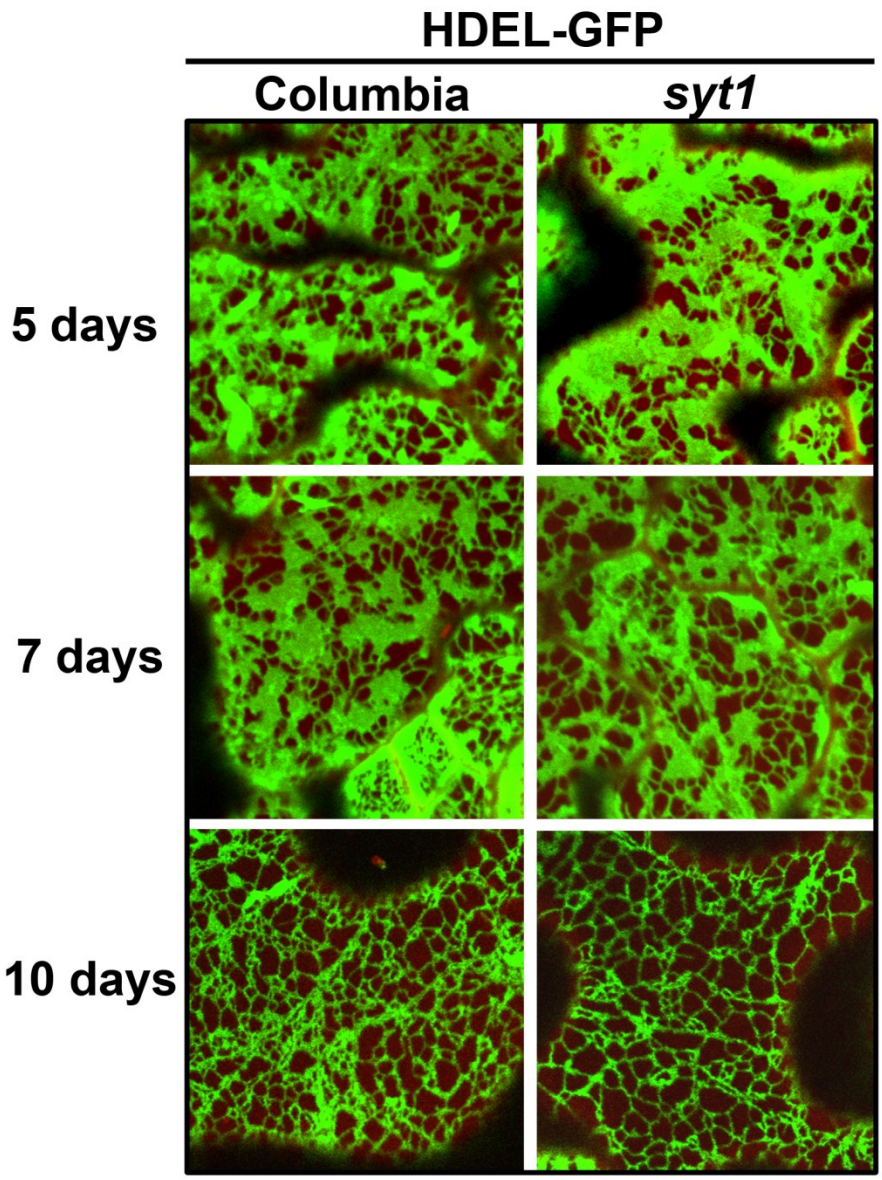

Figure S11. The gross ER morphology is not affected by the *syt1* mutation. Representative images of the WT and *syt1* cortical ER signals at different time points are shown.

Supplemental References

Bolte S, Talbot C, Boutté Y, Catrice O, Read, ND, Satiat-Jeunemaitre, B (2004) FM dyes as experimental probes for dissecting vesicle trafficking in living plant cells. *J. Microsc.* **214:** 159–173.

daSilva LL, Snapp EL, Denecke J, Lippincott-Schwartz J, Hawes C, Brandizzi F (2004) Endoplasmic reticulum export sites and Golgi bodies behave as single mobile secretory units in plant cells. *Plant Cell* **16:** 1753–1771.

Wu FH Wu FH, Shen SC, Lee LY, Lee SH, Chan MT, Lin CS (2009) Tape-Arabidopsis Sandwich - a simpler Arabidopsis protoplast isolation method. *Plant Methods* **5:** 16.